Removal of Chromium (VI) from Aqueous solution using Activated Carbon derived from Co-Pyrolytic biochar of Biomass and Waste Tire

By

Usama Jamil

(00000317656)

Supervisor: Dr. Muhammad Zeeshan Ali Khan

Institute of Environmental Sciences and Engineering,

School of Civil and Environmental Engineering,

National University of Sciences and Technology

Islamabad, Pakistan

(2022)

Removal of Chromium (VI) from Aqueous solution using Activated Carbon derived from Co-Pyrolytic biochar of Biomass and Waste Tire

By

Usama Jamil

Registration No. 00000317656

A thesis submitted in partial fulfillment of the requirements for the degree of

Master of Science

in

Environmental Engineering

Institute of Environmental Sciences and Engineering,

School of Civil and Environmental Engineering,

National University of Sciences and Technology

Islamabad, Pakistan

(2022)

APPROVAL CERTIFICATE

Certified that the contents and forms of the thesis entitled “Removal of Chromium (VI) from Aqueous solution using Activated Carbon derived from Co-Pyrolytic biochar of Biomass and Waste Tire” submitted by Mr. Usama Jamil has been found satisfactory for partial fulfillment of the requirements of the degree of Master of Science in Environmental Engineering.

Supervisor: _____

Dr. Muhammad Zeeshan Ali Khan

Associate Professor

IESE, SCEE, NUST

GEC Member: _____

Dr. Muhammad Ali Inam

Assistant Professor

IESE-SCEE, NUST

GEC Member: _____

Dr. Zaeem Bin Babar

Assistant Professor

IESE-SCEE, NUST

THESIS ACCEPTANCE CERTIFICATE

It is certified that the contents and forms of the thesis entitled **"Removal of Chromium (VI) from Aqueous solution using Activated Carbon derived from Co-Pyrolytic biochar of Biomass and Waste Tire"** submitted by Mr. Usama Jamil, Registration No. 00000317656 found complete in all respects as per NUST Regulations, is free of plagiarism, and mistakes and is accepted as partial fulfilments for award of MS degree. It is further certified that necessary modifications as pointed out by GEC members of the scholar have been included in the said thesis.

Supervisor: _____

Dr. Muhammad Zeeshan Ali Khan

Associate Professor

IESE, SCEE, NUST

Head of Department:_____

Dated:_____

Dean/Principal:_____

Dated:_____

DECLARATION

I certify that this research work titled **"Removal of Chromium (VI) from Aqueous solution using Activated Carbon derived from Co-Pyrolytic biochar of Biomass and Waste Tire"** is my own work. This work has not been presented elsewhere for evaluation. The material that has been used from other sources as been properly acknowledged.

_____

Usama Jamil

00000317656

PLAGIARISM CERTIFICATE

I certify that this research work titled as “Removal of Chromium (VI) from Aqueous solution using Activated Carbon derived from Co-pyrolytic biochar of Biomass and Waste Tire” is my own work. Thesis has significant new work as compared to already published or under consideration to be published elsewhere. The thesis has been checked using TURNITIN and found within limits as per HEC plagiarism Policy and instructions issued from time to time.

Usama Jamil Signature:_____

00000317656 Supervisor:_____

Date:_____

DEDICATION

"Dedicated to my exceptional parents, adored siblings, and my friends whose tremendous support and cooperation led me to this wonderful accomplishment".

ACKNOWLEDGEMENT

First and foremost, I acknowledge that it is by the grace of Allah Almighty that I have been able to complete this manuscript. All respect to the Holy Prophet (P.B.U.H) whose life is the model I am trying to base my life around.

Next, I express my utmost thanks to my supervisor Dr. Muhammad Zeeshan Ali Khan, who has supported and guided me throughout my research. His keen interest and valuable suggestions have helped me overcome all obstacles encountered during my research work. I will forever be thankful for his incredible guidance, encouragement, and sympathetic attitude during the entire period of my research. I am also thankful for the meaningful advice and inspiring attitudes of Dr. Muhammad Ali Inam and Dr. Zaeem Bin Babar which encouraged me to work harder during my research.

This acknowledgement would be incomplete if I do not pay my sincere and heartedly thanks to my cherished and loving parents for their sacrifices, prayers, and affections without which it would have been nearly impossible to achieve my goals. My sincerest thanks to all my friends at IESE specially Usama Khalid & Amir Younus for their support and help during my MS course at NUST. I would also thank other institutes for their continuous support and encouragement throughout my time at NUST. Last but not the least I would like to thank all the laboratory staff at IESE for their help and cooperation.

Usama Jamil

TABLE OF CONTENTS

LIST OF ABBREVIATIONS

WS	Wheat Straw
WT	Waste Tire
AC	Activated Carbon
CAC	Commercial Activated Carbon
LAC	Lab grade Activated Carbon
WHO	World Health Organization
PZC	Point of zero charge
PFO	Pseudo first order
PSO	Pseudo second order
WSBC	Wheat straw biochar
WTBC	Waste tire biochar
MEMF	Micellar-enhanced microfiltration
PEUF	Polymer-enhanced ultrafiltration
DFT	Density Function Theory

LIST OF TABLES

LIST OF FIGURES

Abstract

Biochar derived from Wheat Straw (WS), Waste Tire (WT), and their combination of 1:1 (WS/WT) was activated by different chemical activation methods i.e., wet activation (Molar solution of KOH and Biochar) and dry activation (Physical mixing of Biochar and KOH). Moreover, the synthetized adsorbents were characterized by SEM-EDS, FTIR, BET, XRD and Point of Zero charge (PZC). Efficient adsorbent from both the methods was selected based on the results of characterization and removal efficiency for Chromium (VI). It indicated that WSKOH 1:3 prepared from dry activation method possess well developed porous structure, abundant active sites, and larger specific surface area (529.48m^2/g), auspicious for the elimination of Chromium (VI). The effect of adsorbent dosage, pH, contact time, initial pollutant concentration, and temperature on the efficient adsorbent was also investigated. The batch adsorption studies revealed that WSKOH 1:3 had the highest Chromium (VI) removal at PH 2.0 and contact time of 120 minutes. The Pseudo-second order (PSO) kinetic model and the Freundlich Isotherm model well defined the removal of Chromium (VI), indicating that chemical adsorption predominated the adsorption process. The maximum Langmuir adsorption capacity (q_{max}) of WSKOH 1:3 at 25^{o}C was 96.082 mg/g, which is comparable to other studies. The thermodynamic analyses revealed that Chromium (VI) uptake is endothermic (+ΔH) and spontaneous (-ΔG) in nature. Furthermore, electrostatic attraction, complexation, ion exchange, and reduction to chromium (III) were involved in the removal of chromium (VI) by WSKOH 1:3. Hence, the results proposed that WSKOH 1:3 exhibited great potential for chromium (VI) adsorption.

CHAPTER 1

INTRODUCTION

1.1 Background

Chromium (Cr) is a heavy metal commonly used in industrial processes such as steel production, textile dyeing, metal smelting, tanning, and paints. In the natural environment, chromium can be found in a variety of oxidation states ranging from +2 to +6, however, Cr (III) and Cr (VI) are the most ubiquitous among all (Md Aminul Islam et al., 2019). Industries that use Cr (VI) include leather tanning, mining, wood preservation, textile printing and dying, paints and pigments, aerospace, and electroplating (Ren et al., 2017). The primary reason for the release of Cr (VI) into the environment include the improper disposal practices associated with industries. According to the World Health Organization (WHO), the maximum allowable limit of Cr (VI) in water is 0.05 mg/L, while the United States Environmental Protection Agency (USEPA) recommends 0.1 mg/L in inland surface water (Md Aminul Islam et al., 2020). Therefore, it is critical to select an appropriate and profitable Cr (VI) removal technology.

Various methods utilized for heavy metal removal from wastewater include ion exchange, electrochemical treatment, membrane separation, precipitation, and adsorption. However, most of the technologies have technical and economical limitations for instance incomplete removal of metals, production of sludge and high energy requirements which impede their widescale development and commercialization (J. Zhao et al., 2020a). For practical application, adsorption method seems to be most feasible wastewater treatment technology owing to its environmental and economical sustainability (Alshameri et al., 2018). The adsorption process necessitates a low cost and highly efficient adsorbent with high removal proficiency and high adsorption capability under various conditions (N. Zhao et al., 2017a). Commercially available Activated Carbon (AC) are commonly used as adsorbent, but the most important drawback of these adsorbent is the high production cost (Amen et al., 2020). Biochar, which is synthetized by pyrolyzing various biomass, has specific surface properties, and can be used as an inexpensive adsorbent for heavy metal removal (X. Zhang et al., 2018). Therefore, biochar is considered as a cost-effective and energy effective alternate of AC for pollutant.

Biomass is available in abundance and is regarded as the world's largest source of renewable energy (Farooq et al., 2018). Wheat straw (WS) is the second most abundant biomass type, trailing only rice straw (Neshat et al., 2017). Wheat is widely grown crop and is cultivated in over 115 countries. . WS is used in animal feed in part, but its large production causes assortment and dumping issues. Likewise, the automobile industry is growing rapidly due to modernization and improved lifestyle across the globe. Annual manufacturing of tire is around 1.4 billion units which is equal to 17 million tons of waste tire per year (Acosta et al., 2016). Consequently, the waste tires production and their disposal are a global environmental challenge. The valorization of agricultural residues and waste tire to produce high carbon biochar and activated carbon is an intriguing subject among global researchers. Various biomass types such as corn straw (H. Ma et al., 2019), rice husk (Agrafioti et al., 2014), and sawdust (Garg et al., 2004) have been utilized as pyrolysis feedstock. Biochar produced from pyrolysis of feedstock have been extensively used for adsorption purposes due to its cost-effective and environment friendly nature. Unfortunately, biochar acquires small specific surface area that affect its adsorptive performance (Qu et al., 2021). Hence, activation of biochar by physical and chemical methods are commonly used to improve adsorptive efficiency of biochar (Dias et al., 2020).

1.2 Problem Statement

Growing industrialization and urbanization have posed a significant threat to the quality of groundwater. A potential environmental and public health concern for millions of people worldwide is groundwater contamination with chromium metal from the tanning and leather industry. In natural environment, chromium occurs as Chromium (III) and Chromium (VI), while Chromium (VI) is more solvable and perilous than Cr (III). Cr (VI) can cause stern health issues like lungs damage, skin irritation and even cancer.

On the other hand, large potential of agriculture biomass is burnt every year which directly effects environment and human health. Wheat crop is cultivated in many areas of Pakistan and the surplus of wheat residue (wheat straw) is considered as waste. Proper handling is required to manage the surplus of wheat residue. Literature survey shows, unsatisfactory handling practices creates problems and create negative effect on the environment. Consequently, its utilization in the form of biochar via

pyrolysis can be a valuable process. This study is carried out to prepare a low-cost activated carbon derived from pyrolytic biochar of WS, WT, and their 1:1 combination, i.e., (WS/WT)BC, for the removal of Cr (VI). Adsorption, as opposed to traditional methods, is a sustainable and profitable method for the management of toxic elements such as chromium.

1.3 Research Objectives

The main objectives of this research work are

- Production, Activation, and Characterization of Biochar
- Evaluation of Chromium (VI) removal efficiency and adsorbent removal capacity using batch experiments.

CHAPTER 2

LITERATURE REVIEW

2.1 Background

One of the major concerns facing the world today is environmental pollution. Many countries along with Pakistan are facing this problem due to ever growing population rate, consumption of natural and synthetic resources, industrialization, and heavy dependency on fossil fuels. Every aspect of our life contributes to air pollution, water contamination or soil pollution one way or the other. Rapid industrialization is a major contributor to water pollution.

Water is considered as an essential commodity for sustaining life and environment that is always thought to be an inexhaustible resource. In this new era, over eight billion humans, is facing a serious water crisis. Pakistan is a water stressed country, with per capita water accessibility of only 930 m3 annually. Rapid industrialization and urban development, along with increasing irrigation needs for agriculture, are depleting both the quantity and quality of the country's water resources, have negative impact on the agricultural output and the health of the population (WWF, 2021). The effluent released, contaminates freshwater bodies like rivers, lakes, and fresh underground water reservoirs. This renders the water unsuitable for domestic usage.

Toxic metals in the environment are a worldwide concern due to their negative impacts on humans and aquatic flora and fauna. Heavy metal dumping to the soils and water causes substantial environmental risks due to its non-decomposable nature (Agrafioti et al., 2014). Arsenic (X. Sun et al., 2021), Lead (Das et al., 2021), and Chromium (T. Li et al., 2021) are among the most toxic heavy metals. Researchers around the world are focusing to remove or reduce the concentration of these heavy metals from wastewater up to acceptable limits.

2.2 Introduction of Chromium

Chromium is a heavy metal that displays several properties depending on its valence states, chromium (III), a trace element, is crucial for human body in contrast hexavalent chromium (VI) is lethal and oxidative (Hayashi et al., 2021). Chromium and its compounds are mainly utilized in, metallurgy, and pigments. Effluents from

these industries are disposed into rivers, ponds, and oceans and directly effecting living organisms due to its carcinogenic and mutagenic nature. Exposure of heavy metals like chromium even in small concentrations is hazardous and its removal is still a challenging task for modern researchers.

2.3 Sources of Chromium

Chromium compounds are only noticed in trace amounts in water; however, the element and its compounds can be disposed into surface water by a variety of industries. Chromium is present in both natural and man-made sources. Geological ultramafic and basaltic rocks, especially serpentinites, are natural sources; these rocks are frequently replaced by amphiboles, garnets, micas, pyroxenes, and spinel. Man-made sources include tanneries, metal finishing, cooling towers, pigment synthesis, dyeing, and chemical industries that use high chromium salts (Kanagaraj & Elango, 2019).

2.4 Application of Chromium

Chromium oxide (Cr2O3) has become a widespread material for research purposes due to its superb physicochemical properties. Chromium is used to tint glass emerald, green. Chromium compounds are used as mordents in the textile industry, as well as anodizing aluminum in the aerospace and other industries. Because of its high melting point, medium thermal expansion, and crystalline structure stability, chromite has been used in the refractory industry to form bricks and shapes. Chromium is employed in alloy fabrication, alloy steel preparation to improve corrosion and heat resistance, nonferrous alloy manufacturing to impart special qualities to the alloys, insoluble salt production and processing, and moth proofing wool (Babu et al., 2019). According to the arrangement of the glass and the melting condition, Cr3+ and Cr6+ ions can coexist in silicate and borate glasses in varying ratios (Marzouk et al., 2013). The main function of Chromium in the body is to regulate blood flow, moderate cholesterol levels, contribute to lean muscle mass, promote arterial health, boost the immune system, and stimulate protein synthesis (Costa, 2003).

2.5 Effects of Chromium

Cr (III) is required by plants, whereas Cr (VI) is toxic to both plants and animals at low concentrations. Because Cr (III) oxides are only marginally soluble in water, their concentration in water sources is constrained. Under aerobic conditions,

hexavalent chromium compounds are stable, but under anaerobic conditions, they are reduced to Cr (III) compounds. In an oxidizing environment, the reverse process is also a possibility. Chromium concentrations in soils ranging from 500 to 6000 mg/L are not harmful to plants (Mohamed et al., 2020). Chromium toxicity has a pH-dependent mechanism. Chromium availability to plants is reduced as soluble chromates are converted to insoluble Cr (III) salts. This mechanism safeguards the food chain against excessive chromium levels (Sanyal et al., 2015). Cr (VI) is a poison that is easily absorbed and can be swallowed or inhaled. Skin contact with Cr (VI) can cause vulnerable and genetic defects, as well as cancer, by raiding the respiratory track (Mohamed et al., 2020). High chromium concentrations due to the disposal of metal products in surface water can affect the gills of fish swimming near to the disposal site (Wionczyk et al., 2006).

2.6 Technologies for Cr (VI) Removal

Technologies for Cr (VI) removal include (Karimi-Maleh et al., 2021).

- Ion exchange
- Electrocoagulation
- Photocatalysts
- Membrane technology
- Adsorption

2.6.1 Ion Exchange

The ion exchange is known physicochemical method that implies the replacement of ions between solids and liquids (Hu et al., 2020). and has great success for the removal of Cr (VI). Cr (VI) was removed from water using a variety of ion exchange resins. These resins are composed of a matrix, a three-dimensional molecular network having chemically bonded charged functional groups. Sapari et al. (1996) considered the removal of Cr (VI) from real plating wastewater using synthetic ion exchange resin (Dowex 2-X4) and achieved 100% results. Use of IRN77 and SKN1 cation resins for removal also shows effective results and remove 95% Cr (VI) from water. Adsorption capacities for both IRN77 and SKN1 were 35.38 and 46.34 mg/g respectively (Rengaraj et al., 2001). Some of the important parameters for ion exchange method include resin dose, pH, and initial Cr (VI) concentration (Fu et al., 2013).

The main drawbacks of this process are

- Other competing ions like sulphate, carbonate, phosphate reduces the removal efficiency.
- The cost of resin, waste disposal and regeneration make the process expensive.
- Treated water contains high level of chlorides.

2.6.2 Electrocoagulation

Electrocoagulation (EC) is an effective method for eliminating impurities from water that involves passing an electric current through metal plates to subvert fine material and counteract the electric charge of impurities, causing them to coagulate (Nidheesh et al., 2021). A relatively small reactor is required for confined wastewater at low temperature and turbidity. The flocks formed in EC are more stable and resistant to acids when compared to chemical coagulation; however, when aluminum or aluminum sulphates are used in EC, its efficiency for Cr(VI) removal increases 3 times as compared to chemical coagulation (Golder et al., 2007). Two phases involve for the treatment of Cr (VI) includes (W. Jin et al., 2016).

- Reduction to Cr (III)
- Cr (III) parting as hydroxide

2.6.3 Photocatalysts

Photocatalysts, which produce no harmful chemicals, are another highly effective and cost-effective method for reducing Cr (VI) (Farooqi et al., 2021). Attempts have been made to find an extremely effective photocatalyst for Cr (VI) reduction when exposed to UV, solar, and especially visible light (Liu et al., 2020). Some photocatalysts used for this intent include WO3, SnS2, CdS, CuS, and Ag2S (Niu et al., 2020) although these are hindered by slow reduction rates and low efficiency.

2.6.3.1 Titanium dioxide (TiO_2)

Titanium dioxide is a photocatalyst that is commonly used for Cr (VI) reduction due to its low noxiousness, low cost, and exceptional chemical stability. Some of the drawbacks associated with TiO_2 include its narrow band gap energy and difficulty in separation after treatment (D. Chen et al., 2020). Photocatalytic activity of such photocatalysts depend on interfacial reactions. For that purpose, reduction of Cr (VI) includes three steps (L. Li et al., 2017).

- Surface adsorption
- Photo-reduction and
- Surface desorption

The reduction of Cr (VI) over titanium dioxide, zinc oxide, and nickel oxide is affected by several factors such as structure crystallinity, photocatalyst (C. C. Wang et al., 2016), surface area, pH, Cr (VI) initial concentration, catalyst dose (Idris et al., 2011), calcination time and temperature (Yoon et al., 2009).

2.6.4 Membrane Technology

Membrane filtration is another well known, technology used for the treatment of wastewater (Tanhaei et al., 2014) and used for the removal of Cr (VI) from wastewater (Adam et al., 2018). Various type of membranes depending on the pore size are utilized for this purpose include

- Microfiltration
- Ultrafiltration
- Nanofiltration
- Reverse Osmosis

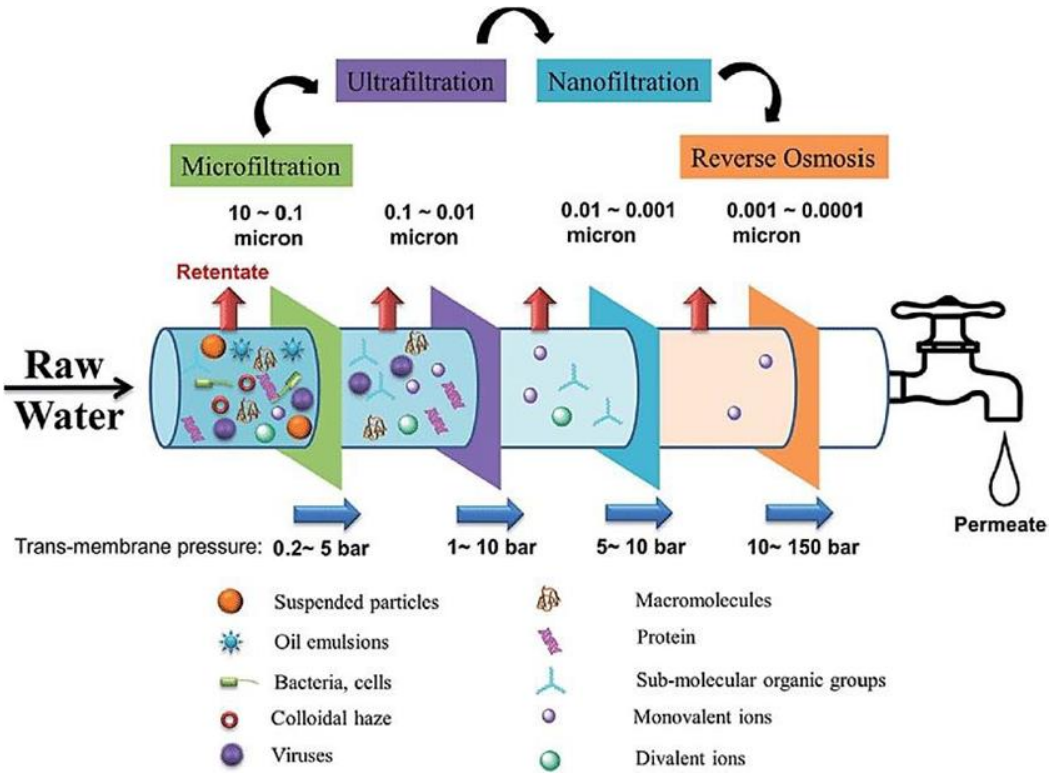

Figure 1: The schematic representation of membrane

2.6.4.1 Microfiltration (MF)

Chromium (VI) ions are smaller in size and are difficult to separate by microfiltration or ultrafiltration. Therefore, a chemical modification is considered necessary to mix Cr (VI) ions with the other massive molecules present (Doke & Yadav, 2014). This problem can be solved by modifying the membrane material (Jana et al., 2010). Doke & Yadav (2014) used micellar-enhanced microfiltration (MEMF) as a surfactant-based membrane with a cationic surfactant of cetylpyridinium chloride. They discovered that the surfactant-to-chromate ratio was 2.5, which was lower than the CMC best ratio for 99% Cr (VI) removal when using a ceramic titania membrane.

2.6.4.2 Ultrafiltration (UF)

Ultrafiltration (UF) is one of the membrane methods that involves the least amount of pressure. The primary use of UF is to split pollutants with high molecular weight, such as peptides and polysaccharides. Because of their small pore size, UF membranes cannot separate ionic species (Yanhong Zhang et al., 2021). Basumatary et al (2016) investigated the exclusion of Cr (VI) in crossflow mode ultrafiltration using MCM-48, MCM-41, and FAU zeolite placed on porous ceramic support UF membranes. When extreme pressure was used, optimal filtration operation was achieved, whereas denial was high when cross flow rate was low. The removal efficiencies of FAU, MCM-41, and MCM-48 membranes were 82%, 75%, and 77%, respectively. Polymer-enhanced ultrafiltration (PEUF) (Haktanır et al., 2017) and micellar-enhanced ultrafiltration (MEUF) (Elfeky et al., 2017) membranes are also utilized for the removal of Cr (VI).

2.6.4.3 Nanofiltration (NF)

Nanofiltration has also been used for the removal of Cr (VI) from wastewater (Wei et al., 2019). NF300 membrane showed higher removal efficiency as compared to PN400 nanofiltration membrane and removed 97% and 92% Cr (VI) and fluoride ions from dual solution respectively (Gaikwad & Balomajumder, 2017). It was noticed that with an increase in pressure, refusal of Cr (VI) and fluoride ions also increased, and it will decrease as the feed concentration increased. The removal of Cr (VI) was also accomplished using a thin film charged surface NF membrane, the surface of which, owing to its negative surface charge, prevents the formation of Cr and other anions (Bohdziewicz, 2000). The results showed an increasing trend as the

pH increased. This is due to membrane surface deprotonation, which increased electrostatic repulsion and the production of CrO_4^{2-}.

2.6.4.4 Reverse Osmosis

The reverse membrane (RO) technology is advantageous for the removal of Cr (VI). RO membranes are operated at high pressures to achieve the highest effluent water purity. Gaikwad & Balomajumder (2017) used polyamide RO membranes to remove Cr (VI) and fluoride ions from aqueous solution. The results showed that increasing the pressure and decreasing the concentration of Cr (VI) and fluoride ions in the feed increased their removal. When the pH of the solution was raised to 8, removal was also increased. Similar results were obtained for Cr (VI) and fluoride ions using the NF500 membrane.

2.6.5 Adsorption

Adsorption is one of the most appropriate, competent, and applicable technology for the removal of heavy metals including Cr (VI) (Yaashikaa et al., 2019). Researchers have been looking for suitable adsorbents having higher removal efficiencies and higher adsorption capacities for the removal of Cr (VI) from polluted water. For that purpose, variety of adsorbents including natural organic, natural inorganics, and synthetic adsorbents have been considered (Pakade et al., 2019). These adsorbents have been used in their original form, but their modification i.e., change in chemical structure, cross linking, and grafting has attracted great attention. Four mechanisms proposed for the interaction between Cr (VI) and adsorbents are (Pakade et al., 2019)

- Adsorption through electrostatic forces
- Cr (VI) reduction to Cr (III)
- Ion Exchange mechanism
- Complex formation

2.6.5.1 Characteristics of an Ideal Adsorbent

The particle size of the adsorbents plays a vital role to improve the adsorption efficiency (Hamadi et al., 2001). The important characteristics of an ideal adsorbent are (Bhatnagar & Minocha, 2006).

- Adsorbent has uniform pore structure

- It has large surface area
- It requires less time to reach equilibrium
- It has high chemical and physical strength

2.6.5.2 Adsorbents used for Cr(VI) removal

Common adsorbents used for the removal of Cr (VI) include (M. B. Ahmed et al., 2016)

- Activated Carbon (AC)
- Graphene Oxide
- Biochar

Activated Carbon (AC)

Activated carbons (ACs) are the extensively used adsorbents due to its versatile nature i.e., its properties can be modified according to specific objectives. The most important aspects of ACs are the high specific surface area and pore volume that increase contact between adsorbent and effluent to obtain the maximum removal performance. However, the major disadvantage of ACs is its high production cost (Danish & Ahmad, 2018). Fox nutshells-based AC was used for Cr (VI) adsorption from water, and the results showed that the AC produced has a high surface area, the process is endothermic, and the maximum adsorption capacity was found at pH 2 (Kumar & Jena, 2017).

Graphene Oxide

Graphene is a one-atom-thick layer of closely packed covalently bonded atoms of carbon in a two-dimensional honeycomb lattice (Yang et al., 2010). It has distinctive electronic, thermal, and mechanical properties, such as superior mobility of charge carriers, thermal conductivity and has thus been used for sensors supercapacitors , batteries , catalysts , and field-effect transistors (Youwei Zhang et al., 2013). However, Treatment of wastewater through adsorbent prepared from graphene is still a challenge. Ma et al. 2020 prepared a graphene adsorbent with amine group (ED–RGO) from graphene oxide and found that the synthesized adsorbent performed better for the removal of Cr (VI) when the pH of the solution is less than 2.0 (H. L. Ma et al., 2012). .

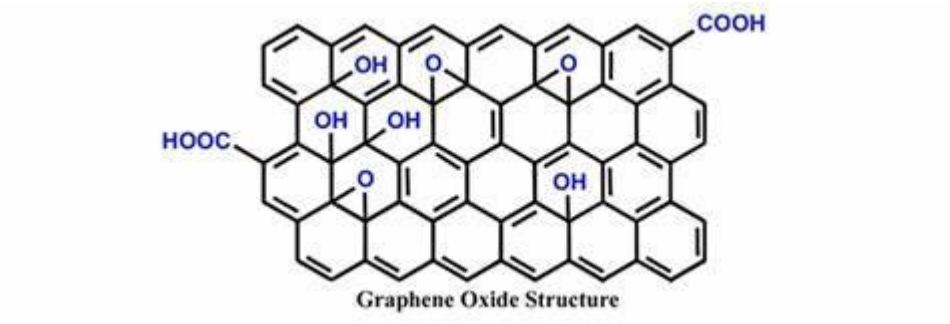

Figure 2: Structure of Graphene Oxide

Biochar

Biochar is usually synthetized from organic feedstocks like industrial and agricultural waste, municipal waste, and algal biomass. It is regarded as an effective adsorbent material due to its excellent adsorption properties for a wide range of pollutants. Functional groups such as carboxylic acids, phenolic hydroxyls, lactones, quinone, carbonyls, ethers, and condensed aromatic rings) present on the surface of the biochar offer active sites for metal adsorption (Herath et al., 2021). Furthermore, using agricultural waste as a feedstock for biochar synthesis aligns with the concepts of sustainable development and the circular economy. Several studies have been carried out to discuss the application of biochar for heavy metal adsorption. Ai et al. (2019) revealed that in acidic conditions adsorption capacity of Cr(VI) by sugar beet tailing biochar reached 123 mg/g (Ai et al., 2019). Corn cobs hydro char modified by polyethylene amine improved the Cr(VI) removal efficiency and the maximum adsorption capacity is 33.663 mg/g (Yuanji Shi et al., 2018). In recent times, there has been a surge of interest in biochar activation, and two methods have been widely used to create porous structures to improve adsorption performance.

- Physical Activation
- Chemical Activation

Physical Activation

Physical activation of biochar is usually done at 900°C with the help of steam or CO_2 (Qu et al., 2021). It entails carbonizing feedstock and then activating the resulting biochar at high temperatures with appropriate oxidizing gases such as carbon dioxide, steam, air, or a combination of these gases (di Stasi et al., 2019). The

activation temperature ranges between 600 and 900^{o}C, and the carbonization temperature ranges between 400 and 850^{o}C, with temperatures occasionally exceeding 1000^{o}C. Physically activated carbon lacked the properties required for use as adsorbents or filters (Ioannidou & Zabaniotou, 2007).

Chemical Activation

Chemical activation has achieved more attention as compared to physical activation due to its economical operating conditions and superior qualities of the products such as higher specific surface area porosity (Aghababaei et al., 2017). The main drawback associated with chemical activation is corrosivity of the equipment. Moreover, the obtained adsorbent requires washing with suitable solvent after activation to remove activating agent (Ioannidou & Zabaniotou, 2007). Commonly used chemical agents for activation include $ZnCl_2$, KOH, H_3PO4 and less K_2CO_3. The production and activation of biochar could be attained in one step or two step technique. Feedstock is mixed with the activating agent and thereafter the mixture is pyrolyzed at suitable temperature in one step technique. Whilst in two step process, the biochar is prepared in the first stage which is then treated with the agent in the second stage. However, two-step process has been considered superior to one step method due higher surface properties of adsorbent synthesized through former (Abbaci et al., 2022). However, the limited literature is available on two step technique, using KOH as an activating agent, to synthesize activate carbon from wheat straw and waste tire to remove Cr(VI).

Keeping the research gap in view, present study investigates the production of biochar from WS, WT and their combination using slow pyrolysis. Furthermore, the activation of biochar has been performed to produce activated carbon using various mixing techniques and ratios of biochar samples and activating agent (KOH). The performance of fifteen biochar and activated carbon samples was investigated by removing the Cr(VI) from the solution while keeping the operating conditions such as pH, contact time and initial concentration similar. Ultimately, the most efficient adsorbent was selected on the grounds of various characterization analysis and experiment which was further used in the adsorption experiments under varying operating conditions. In addition, the kinetics, isotherms, and thermodynamics properties of optimized adsorbent were investigated comprehensively. In addition, the

regeneration of the optimized adsorbent was also performed and the impacts on removal efficiency were investigated accordingly.

CHAPTER 3

MATERIAL AND METHODS

This chapter provides information on preparation of feedstock, synthesis of biochar, activation procedure of biochar , characterization of activated carbons, and removal parameters of Chromium(VI) used in this study. It details out the simulation methods used to quantify the experimental results. It also explains the analytical procedures adopted for the characterization of biochar and activated biochar.

3.1 Feedstock preparation

In this study, wheat straw (WS), a common agricultural byproduct, was calmly sourced from a nearby farm in Rawalpindi, Pakistan. It was sun-dried for one day to reduce the moisture content. It was manually shredded, ground, and sieved to achieve a particle size range of 0.6 to 1.2 mm, as shown in the Figure. 1. Waste tire (WT) was purchased from a local vendor in Lahore, Pakistan. It was shredded, ground, and sieved to achieve the same particle size as WS.

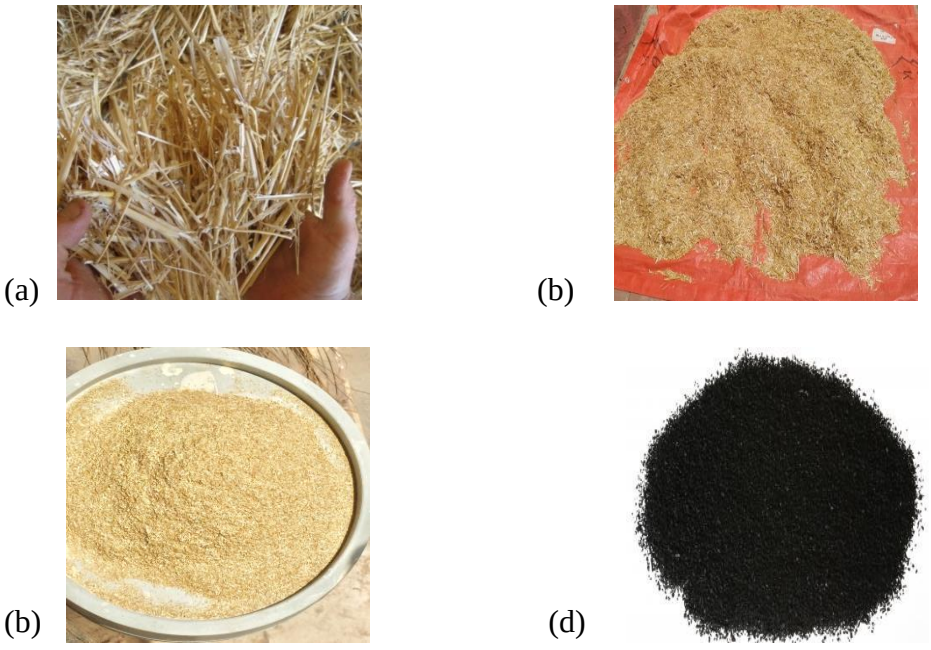

Figure 3: Preparation of Feedstock (a) Raw wheat straw (b) Shredded form (c) Grinded form (d) Powder waste tire

3.2 Experimental Setup and Pyrolysis Procedure

The components of experimental setup used for production of biochar are given in Figure 3.2. The setup contains

- Fixed Bed reactor
- Condenser
- PID temperature controller
- Flow meter for Nitrogen
- Heaters
- Nitrogen cylinder
- Thermocouples

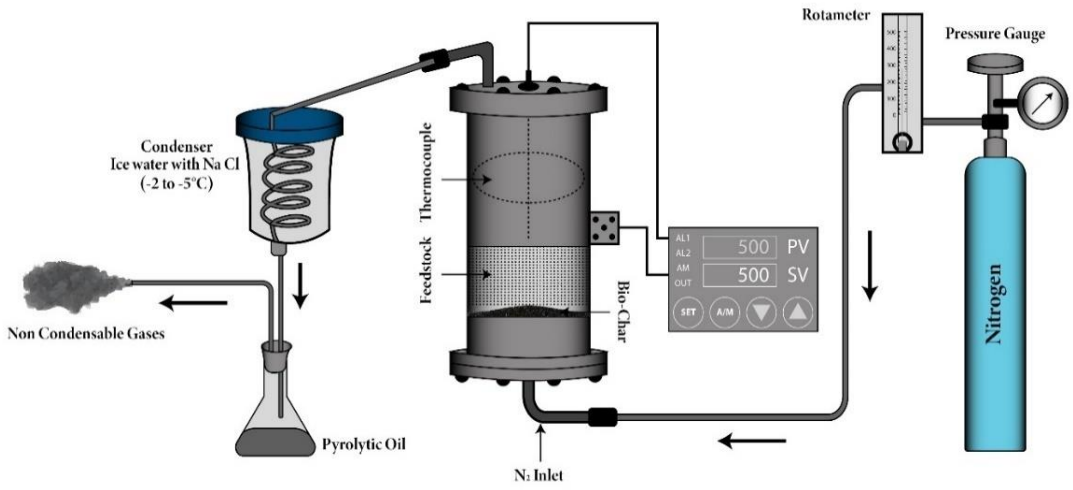

Figure 4: The schematic diagram of experimental setup

The pyrolysis and co-pyrolysis of WS and WT were carried out in a stainless-steel fixed bed reactor with a length of 20 inches and an internal diameter of 4.2 inches, as shown in Figure 2. 100 g of feedstock was fed into the reactor to produce biochar. Biochar was produced using two blend ratios 1:0 and 1:1. All experiments were carried out in triplicate. The reactor was heated at a constant rate of 20^{o}C per minute from room temperature to 550^{o}C until all the oxygenates had been expelled. It usually takes one hour. Nitrogen was introduced as a sweeping gas from the bottom of reactor at a rate of 300 mL/min. Prior to the start of the heating process, N_2 flow was

maintained to purge the air from the reactor. During the pyrolysis process, vapors and gases were removed from the top of the reactor along with N_2. Hot gases were expelled from the ice-covered condenser. The produced oil was collected in a conical flask attached to the condenser. Finally, after the reactor had cooled, the biochar produced was collected. The biochar produced by both blend ratios was designated as WSBC, WTBC, and (WS/WT)BC.

Following the completion of the run, the liquid and biochar quantities acquired were weighted, and the amount of gas produced was determined by subtracting the initial sample weight from the total weight of liquid and char produced.

3.3 Activation of Biochar

In this study, the biochar produced from pyrolysis of WS, WT, and their combination of 1:1 i.e., (WS/WT)BC was activated by chemical activation.

3.3.1 Activation method

Two step activation method was used in this study. Potassium Hydroxide (KOH) was used as chemical activator. The activation methods are as follows.

- Wet Activation
- Dry Activation

3.3.1.1 Wet Activation

For Wet activation, biochar i.e., WSBC, WTBC, and (WS/WT)BC and two concentrations of KOH (1M, 3M) with a ratio of 1:100 (w/v) were mixed and stirred at 60^{o}C for 2 hours. The liquid part was filtered, and BC dried overnight at 105^{o}C. After this, the chemically treated biochar was heated at 700^{o}C in a reactor under inert atmosphere for 1 hour at a heating rate of 10^{o}C/min. The activated biochar thus obtained were named as WS-KOHx, WT-KOHx, and WS/WT-KOHx where x represents the concentration of KOH.

3.3.1.2 Dry Activation

For Dry activation, biochar was physically blended with two BC to KOH mass ratios (1:1 and 1:3). And introduced into the pyrolysis reactor for 1 hour at 700^{o}C under inert atmosphere at a heating rate of 10^{o}C/min. The activated biochar thus

obtained were named as WSKOH-r, WTKOH-r, and WS/WTKOH-r where r represents the impregnation ratio.

Nitrogen was used as an inert gas to purge the air from the reactor at a rate of 100 ml/min. Finally, the activated adsorbents from both activation methods were washed first with 1M HCl and then with deionized water to normalize pH and placed in oven for drying at 105^{o}C for 24 hours.

3.4 Characterization of biochar and Activated biochar

Raw biochar and chemically activated biochar of WS, WT, and WS/WT were characterized by number of analytical techniques to evaluate the effect of chemical addition with biochar. Following section describes the experimental procedure with some theoretical background for each technique.

3.4.1 Proximate Analysis

Raw and Activated biochar were tested for proximate analysis via ASTM standard D3173, D3174, D3175 for Moisture content, Volatile matter, Ash content, and Fixed carbon respectively.

To determine moisture content measured samples were placed in oven for 24 hours at 105^{o}C. After oven drying, samples were removed from the oven and difference in the weight give moisture content. For volatile matter measured samples were placed in crucibles with caps and placed in muffle furnace for 7 minutes at 950^{o}C. After completion of time samples were taken out and difference in the weight of samples give volatile matter. For Ash content samples were placed in crucibles with lid and placed in muffle furnace at 725^{o}C for 3 hours. After the specified time samples were taken out and the weight difference give the ash content. Fixed carbon in raw and activated biochar was determined by the difference of moisture content, volatile matter, and ash content from 100.

3.4.2 Ultimate Analysis

Concerning the elemental analysis, CHNS were quantified with CHN analyzer (Perkin Elmer 2400). Oxygen percentage was intended by difference in the values of C,H,N,S and ash content from 100. 80 mg of each sample was used to perform this analysis.

3.4.3 BET Analysis

Surface textural properties of all the adsorbents were determined using adsorption-desorption isotherms of nitrogen at 77 K acquired through Surface Area & Pore size analyzer (NOVA 2200e, Quantachrome Instruments). Before performing experiments, all the adsorbents were degassed overnight to remove the moisture. The degassing temperature was set at 150^{o}C. Multipoint method was used to determine the BET Surface area (S_{BET}). To identify the type of isotherm, isotherms for all adsorbents were plotted between relative pressure p/po = 0.99 and quantity of N_2 adsorbed in cm^3/g. Pore volume was determined by the amount of N_2 adsorbed at a relative pressure of p/po = 0.99. Pore size distribution data obtained from density function theory (DFT) method was used to calculate the average pore width and to plot the pore width against quantity of N_2 adsorbed in cm^3/g.

3.4.4 SEM-EDS Analysis

Surface morphology of the raw and activated samples were analyzed by scanning electron microscopy along with energy dispersive spectroscopy (51-ADD007, Oxfords Instruments). To acquire the SEM images the acceleration voltage was set as 20 kV. And different magnifications i.e., 10X, 100X, 1000X was used.

3.4.5 Fourier Infrared Spectroscopy (FTIR)

Functional groups on the surface of adsorbents were determined by using Fourier infrared spectroscopy (FTIR; Bruker Spectrum 400 spectrometer). The KBr disk method was used for this purpose having wavenumber ranged from 4000 to 400 cm^{-1}, with a resolution of 1 cm^{-1}.

3.4.6 Powder X- ray Diffraction (XRD) Spectroscopy

Crystal structures were analyzed by X-ray diffractometer (θ-θ STOE Germany). Diffractograms were acquired with continuous scanning from 10 to 80^{o} (2θ) with a step size of 0.04^{o} (2θ). The crystallinity of all the samples were calculated by using the equation

$$\text{Crystallinity} = \frac{\text{area of crystalline + amorphous peaks}}{\text{Total area of crystalline + amorphous peaks}} * 100$$

Phase identification was measured using X`Pert High Score Plus software. The degree of crystallinity was determined based on characteristic peak`s intensity at 2θ.

3.4.7 Point of Zero Charge (PZC)

The Point of Zero Charge (PZC) of adsorbents was calculated based on the methodology described by (Mortazavian et al., 2018);(Godinho et al., 2017). 0.1 g of adsorbent was added in 50 mL of 0.1 M NaCl solution in 7 different flasks. Initial pH of NaCl solutions was adjusted to 3.0, 4.0, 5.0, 6.0, 7.0, 8.0, and 9.0 by addition of either 0.1 M HCl or 0.1 M NaOH. The samples were placed on shaker for 24 hours and after the termination of time final pH of samples were calculated using a pH 700, pH/mV/^{o}C/^{o}F meter. The PZC was determined by a plot between Initial pH and Equilibrium pH.

3.5 Adsorption Experiments

The Cr (VI) stock solution (1000 mg/L) was prepared by dissolving potassium d ichromate ($K_2Cr_2O_7$) in distilled water.

3.5.1 Selection of Efficient Adsorbent

To select the most efficient adsorbent, adsorption experiments were carried out by shaking 0.1 g of adsorbent with 100 mL of Cr (VI) solution at 150 rpm. The initial concentration of Cr (VI) was 20 mg/100 mL. After filtration, the final concentration of Cr (VI) was determined by UV-Spectrometer (Specord 200 plus Germany). Removal efficiency (%) and adsorption capacity (mg/g) of the adsorbent was calculated as

$$R(\%) = \frac{C_o - C_f}{C_o} * 100 \qquad (1)$$

$$q_e\left(\frac{mg}{g}\right) = (C_o - C_f) * \frac{V}{m} \qquad (2)$$

where C_o (mg/L) and C_f (mg/L) represent the initial and final concentration of Cr (VI) respectively. V (L) is the volume of solution and m is the mass of adsorbent.

After selection of efficient adsorbent, batch experiments were performed on the efficient adsorbent to optimize the experimental parameters i.e., adsorbent dosage, pH, contact time, initial concentration, and temperature.

3.5.2 Optimization of Experimental Parameters

To optimize the experimental parameters for the removal of Cr (VI), all the parameters were varied one by one keeping the other parameters constant.

Effect of adsorbent dosage was determined by varying the dosage from 0.5 to 7 g/L. Other parameters include initial concentration of Cr (VI) 100 mg/L, pH 2.0, contact time of 120 minutes, temperature 25^{o}C and RPM 150.

Effect of pH was investigated by varying the pH value from 1.5 and 9. Other parameters include the initial concentration of Cr (VI) 100 mg/L, adsorbent dosage 2 g/L, contact time of 120 minutes, temperature 25^{o}C and RPM 150.

Effect of contact time was varied from 0 to 360 minutes during which samples were analyzed at different time intervals (5, 15, 30, 60, 90, 120, 180, 240, 300, and 360 minutes). Other parameters include the initial concentration of Cr (VI) 100 mg/L, adsorbent dosage 2 g/L, pH 2.0, temperature 25^{o}C and RPM 150.

Effect of initial Cr (VI) concentration and temperature was investigated by varying the initial concentration of Cr (VI) i.e., 10, 20, 50, 100, 150, 200, and 250 mg/L and temperature 25^{o}C, 35^{o}C, and 45^{o}C respectively. Other parameters include adsorbent dosage 2 g/L, pH 2.0, contact time 120 minutes, and RPM 150.

For comparison purpose, two commercially available activated carbons, commercial activated carbon (CAC) and lab grade activated carbon (LAC) were also analyzed under optimized conditions.

3.5.3 Adsorption Kinetic Studies

To quantitatively assess the trap of Cr (VI) by adsorbent, two well recognized kinetic models, i.e., Pseudo-first order (PFO) kinetic model and Pseudo-second order (PSO) kinetic model were used

$$q_t = q_e(1 - e^{-k_1 t}) \quad (3)$$

$$q_t = \frac{q_e^{2} * k_2 * t}{1 + q_e * k_2 * t} \quad (4)$$

in which q_e (mg/g) and q_t (mg/g) represent the amount of Cr (VI) adsorbed at equilibrium and at time t, respectively. K_1 (min^{-1}) and k_2 (g/mg/min) are the respective rate constants.

3.5.4 Adsorption Isotherm Studies

Two well-known isotherm models, i.e., Langmuir Isotherm model and Freundlich Isotherm model were employed to quantify the adsorption data. These models predict the single and multilayer adsorption respectively.

$$q_e = \frac{q_{max} * K_L * C_e}{1 + K_L * C_e} \quad (5)$$

$$q_e = K_F * C_e^{1/n_F} \quad (6)$$

in which q_{max} (mg/g) represents the uptake capacity of adsorbate onto the adsorbent. K_L represent the energy constant,$1/n_F$ is the coefficient related to sorption intensity, and K_F is the coefficient correspond to adsorption capacity (mg/g).

3.5.5 Thermodynamic Parameter

To further investigate the influence of temperature on adsorption capacity, the thermodynamic parameters (ΔG°, ΔH°, ΔS°) were estimated by using these equations.

$$\Delta G° = \Delta H° - T\Delta S° \quad (7)$$

$$\Delta G° = -RT \ln k_c \quad (8)$$

$$K_c = {q_e}/{c_e} \quad (9)$$

$$\ln K_c = -\left({\Delta H°}/{R.T}\right) + {\Delta S°}/{R} \quad (10)$$

where, T (k) is the absolute temperature, R (J/(mol.k)) is the universal gas constant, k_c (L/g) is the equilibrium constant, and ΔG°, ΔH°, ΔS° represent the standard free energy, enthalpy, and entropy changes respectively.

3.5.6 Regeneration Studies

Regeneration experiments were also implemented after adsorption of Cr (VI) onto the adsorbent. The Cr (VI) packed adsorbent was compiled by filtering the adsorption experiment suspension and then placed in 1M NaOH solution for desorption while being meticulously stirred for 12 hours. After stirring, the adsorbent was separated from the NaOH solution and washed numerous times with distilled water before being dried overnight at 105ºC. Adsorption experiments were performed as described earlier. The adsorption-desorption experiments were performed several times.

CHAPTER 4

RESULT AND DISCUSSION

4.1 Characterization of Raw and Activated biochar

The characterization of all the raw and activated biochar samples were performed and the results are presented here. Characterization of commercial ACs were also performed and presented.

4.1.1 Proximate Analysis

Raw biochar (WSBC, WTBC, (WS/WT)BC) was largely comprised of fixed carbon followed by volatile matter, and ashes content (Table 1). Among all char samples, WTBC has the highest fixed carbon which is attributed to higher fixed carbon content in WT feedstock (Khan et al., 2020). On the other hand, ash content is highest in WSBC which associated with the composition of WS feedstock. Agriculture residues are constituted of metallic content that contributes to ash formation (Khan et al., 2021). Moreover, the highest volatile content in WSBC might be an indication of inefficient decomposition of WS compared to WT during pyrolysis. It is pertinent to mention that the volatile content, calculated through characterization, in co-pyrolytic char (WS/WT)BC) was lower than its theoretical calculated value using rule of mixture. Similarly, the fixed carbon content (70.20) was also higher than the theoretical calculated value (57.80). These observations testify the synergistic reactions between the two feedstocks leading to enhanced decomposition of WS in presence of WT compared to pyrolysis of WS alone. After chemical activation with KOH, volatile matter of WSBC samples decreased from 26.9% in the range (15.6% to 23.81%) and ashes content decreased from 25.5% in the range (10.2% to 17.8%) concentrating the fixed carbon (52.41% to 67.1%). Similar trends were also observed for AC samples of WTBC and (WS/WT)BC) as shown in Table 1. These results are in line with the findings reported by Dias et al. 2020 (Dias et al., 2020). Moreover, the higher activation temperature i.e., 700^{o}C and the increase in concentration of KOH(1:1, 1:3, 1M, 3M) leads to greater loss of volatile matter (Pellera et al., 2012). These results are consistent with BET results as removal of greater fraction of VM increases the surface area specifically for WSKOH 1:3 (Table 3).

Table 1: Proximate analysis of raw biochar and activated carbons (ACs

Adsorbents	Parameters			
	M.C (%)	V.M (%)	Ash (%)	F.C (%)
WSBC	2.2	26.9	25.5	45.4
WTBC	1.6	13.1	15.19	70.20
(WS/WT)BC	1.10	17.6	17.30	64.00
WSKOH 1:1	5.94	18.31	15.23	60.52
WSKOH 1:3	7.10	15.6	10.2	67.1
WS-KOH_{1M}	5.98	23.81	17.8	52.41
WS-KOH_{3M}	9.2	21.0	14.7	55.1
WTKOH 1:1	6.71	11.2	11.25	70.84
WTKOH 1:3	7.08	9.59	6.92	76.41
WT-KOH_{1M}	5.94	11.37	14.19	68.5
WT-KOH_{3M}	7.09	9.65	8.1	75.16
WS/WTKOH 1:1	5.13	15.94	13.23	65.7
WS/WTKOH 1:3	8.73	12.13	11.1	68.04
WS/WT-KOH_{1M}	5.62	16.05	15.07	63.26
WS/WT-KOH_{3M}	9.05	11.27	11.78	67.9

4.1.2 Ultimate Analysis

Elemental analysis of raw biochar (WSBC, WTBC, (WS/WT)BC) and ACs prepared by KOH activation are presented in Table.2. The results indicated that carbon content in WSBC, WTBC, and (WS/WT)BC is 63.24%, 75.21%, and 68.95% respectively. After activation, the carbon content increased (Table 2) revealing that KOH activation accelerated the carbonization of raw biochar. The increase in temperature during activation could be another reason for the increase of relative C content (Shahrokhi-Shahraki et al., 2021). Similarly, the oxygen content also increased indicating that KOH activation increased the oxygen containing functional groups (H. Jin et al., 2014). The aromaticity and polarity of the adsorbents are demonstrated by the H/C and (O+N)/C molar ratios, respectively. The H/C and (O+N)/C values for raw biochar and ACs are also presented in Table 2. The lower H/C values indicate that ACs own high aromaticity and carbonization, making them

efficient adsorbent materials. Similar results were also reported by Qin et al.2022 (Qin et al., 2022). ACs have higher polarity index (O+N)/C as compared to raw biochar, implying that ACs contain more polar functional groups that aid in heavy metal adsorption (N. Zhao et al., 2017b). From Table 2, WSKOH 1:3 acquire higher polarity index (0.314) as compared to other ACs. These results are also supported by FTIR analysis as discussed in section 4.1.5.

Table 2: Elemental composition of Raw Biochar and Activated Carbons

Adsorbents	Parameters						
	C (%)	H (%)	N (%)	S (%)	O[a] (%)	H/C (%)	(O+N)/C (%)
WSBC	63.24	0.77	0.59	0.05	9.86	0.144	0.250
WTBC	75.21	1.81	0.62	2.3	4.87	0.286	0.104
(WS/WT)BC	68.95	1.12	1.75	1.18	9.7	0.19	0.179
WSKOH 1:1	71.07	0.52	1.33	0.73	11.12	0.086	0.251
WSKOH 1:3	73.6	0.24	1.04	0.52	14.4	0.038	0.314
WS-KOH_{1M}	67.28	0.26	1.59	0.67	12.4	0.046	0.296
WS-KOH_{3M}	69.58	0.63	1.68	0.61	12.8	0.107	0.295
WTKOH 1:1	77.36	0.61	0.54	1	9.24	0.093	0.191
WTKOH 1:3	81.21	0.5	0.71	1.2	9.46	0.073	0.187
WT-KOH_{1M}	74.03	0.75	1.33	0.89	8.81	0.120	0.191
WT-KOH_{3M}	78.38	0.9	0.8	1.1	10.72	0.136	0.219
WS/WTKOH 1:1	72.47	0.31	1.88	0.44	11.67	0.050	0.258
WS/WTKOH 1:3	77.76	0.51	1.42	0.21	9	0.078	0.185
WS/WT-KOH_{1M}	69.71	0.71	1.09	0.11	13.31	0.121	0.0.306
WS/WT-KOH_{3M}	74.04	0.51	1.35	0.16	12.16	0.082	0.263

[a]calculated by the difference method

4.1.3 BET Analysis

To optimize the adsorbent for Cr(VI) adsorption, BET analysis of raw and AC samples were conducted prepared by two different methods i.e., wet activation and dry activation. Table 3 shows the physical characteristics of raw and AC samples. The BET surface area (S_{BET}) of WSBC, WTBC, and (WS/WT)BC is 5.37 m^2/g, 20.37 m^2/g and 11.89 m^2/g respectively. After KOH activation at 700^oC, the surface area of samples prepared with wet activation are as follows WS/WT-KOH_{1M} > WT-KOH_{3M} > WS/WT-KOH_{3M} > WT-KOH_{1M} > WS-KOH_{3M} > WS-KOH_{1M}. Whereas, the S_{BET} of dry activation are as follows WSKOH 1:3 > WSKOH 1:1 > WTKOH 1:3, WTKOH 1:1 > WS/WTKOH 1:1 > WS/WTKOH 1:3. The S_{BET} of activated samples are much higher than their respective raw biochar, suggesting that ACs provide greater contact area and more adsorption sites for Cr (VI) adsorption. The total pore volume also increased after activation which could be due to the change in pore size distribution (H. Jin et al., 2014). The increase in S_{BET}, and pore volume after activation indicate that KOH activation is conducive to enhance the surface properties of BCs (He et al., 2019). The WSKOH 1:3 owned the highest surface area (529.48 m^2/g) and pore volume (0.282 cm^3/g) compared to other ACs proposing that WSKOH 1:3 provide greater interaction area and more adsorption sites for the uptake of Cr (VI) (Zhu et al., 2018). Furthermore, the samples prepared with Wet activation possess low surface area (8.22 m^2/g – 41.38 m^2/g) as compared to the values found in literature (Aghababaei et al., 2017). Since most of the previous studies used biomass rather than biochar therefore the hydrophobicity (low atomic O/C value) of the biochar used in this study could explain the low surface area which impeded the diffusion of solution into solid biochar (di Stasi et al., 2019). The O/C values for WSBC, WTBC, and (WS/WT)BC are 0.11, 0.048, and 0.083 respectively. In case of (WS/WT)BC activated samples, the S_{BET} decreased with the increase of KOH concentration (for both activation methods). This could be due to the collapse of structure of (WS/WT)BC at higher KOH concentrations (C. Wang et al., 2021). The S_{BET} CAC and LAC is 819.32 m^2/g and 301.92 m^2/g respectively.

Table 3: N_2 Physical adsorption parameters of Raw and AC samples

Sample	**Parameters**		
	S_{BET} (m^2/g)	Pore Width (nm)	Pore Volume (cm^3/g)
WSBC	5.37	11.44	0.006
WTBC	20.97	3.46	0.0181
(WS/WT)BC	11.89	3.52	0.0129
WSKOH 1:1	134.37	1.85	0.112
WSKOH 1:3	529.48	1.19	0.282
WS-KOH_{1M}	8.22	4.15	0.018
WS-KOH_{3M}	14.84	10.63	0.039
WTKOH 1:1	47.60	12.79	0.235
WTKOH 1:3	79.441	12.8	0.262
WT-KOH_{1M}	16.23	11.69	0.057
WT-KOH_{3M}	28.35	12.0	0.072
WS/WTKOH 1:1	41.38	3.63	0.092
WS/WTKOH 1:3	37.75	2.90	0.087
WS/WT-KOH_{1M}	34.09	12.225	0.083
WS/WT-KOH_{3M}	27.23	12.23	0.068
CAC	819.32	1.06	0.43
LAC	301.91	1.85	0.175

The N_2 adsorption-desorption isotherms are presented in Figure 5. The isotherms of WSKOH 1:3 and WSKOH 1:1 increased speedily at ($P/Po \leq 0.08$) and become horizontal after relative pressure ($P/Po \geq 0.14$) Fig 5(a). Similarly, the isotherm of CAC increased quickly at $P/Po \leq 0.05$ and become horizontal after ($P/Po \geq 0.165$) Fig 5(g). According to IUPAC classification, these trends are consistent with Type I isotherm and suggest that large no. of micropores and some mesopores are present on the surface of WSKOH 1:1, WSKOH 1:3, and CAC (Wu et al., 2022). The H_4 hysteresis loops present in the N_2 adsorption-desorption curves also revealed the existence of narrow pore on the surface of WSKOH 1:1 and WSKOH 1:3 and CAC (Gopinath et al., 2021). Moreover, all other samples of WSBC, WTBC, and

(WS/WT)BC Fig. 5(a,c,e) show Type IV isotherms with H_3 hysteresis rings suggesting that mesopores are present on their surfaces (Qin et al., 2022).

According to Non-Local Density Functional theory (NLDFT), pore size distribution of all samples is presented in Fig 5(b,d,f,h). For WSKOH 1:3 and CAC the pore size is distributed largely in the range 0 - 2.5 nm clearly indicative of the presence of abundant micropores for these samples. Micropores can provide large no. of active sites whereas mesopores could help in heavy metal transfer (H. Ma et al., 2019). The WSKOH 1:1 and LAC also present micropores however are abundant in mesopores Fig. 5(b,h). The pore size for all other samples lies between 2 - 20 nm implying the presence of mesopores. The large surface area of WSKOH 1:3 is comparable to other commercially available ACs typically ranging from 500 to 2000 m^2/g (Duan et al., 2019).

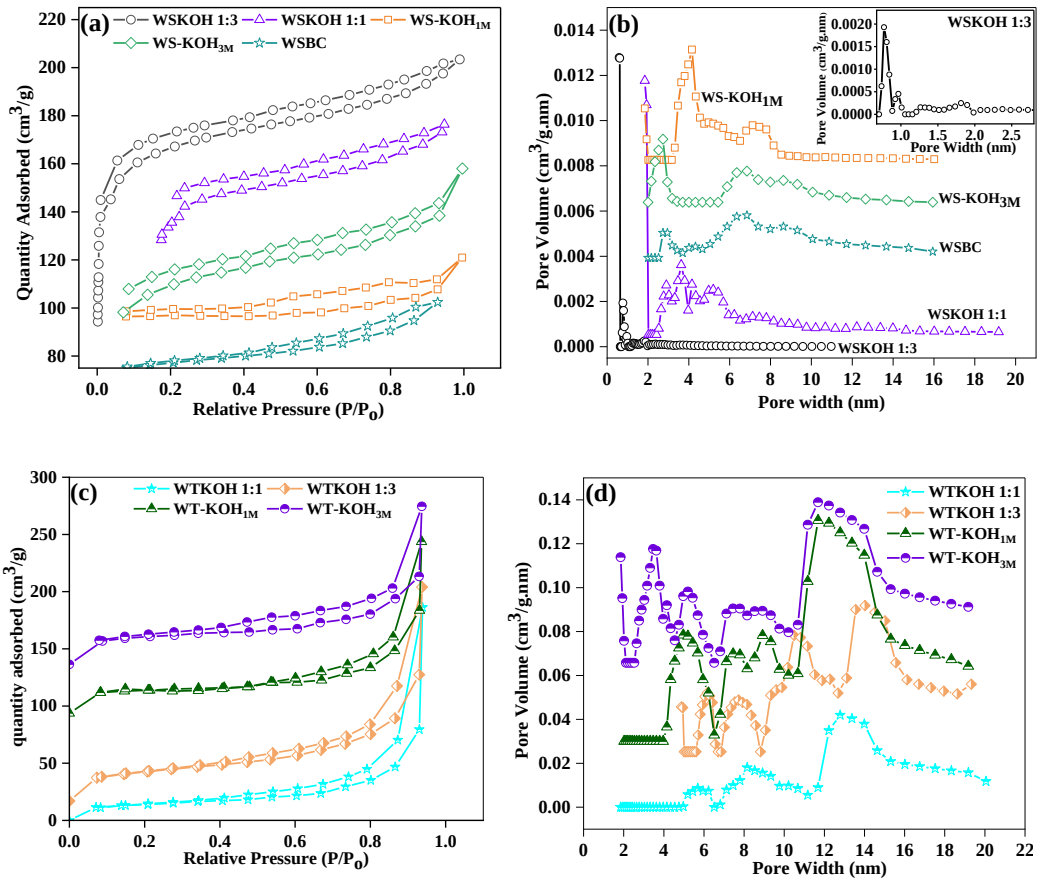

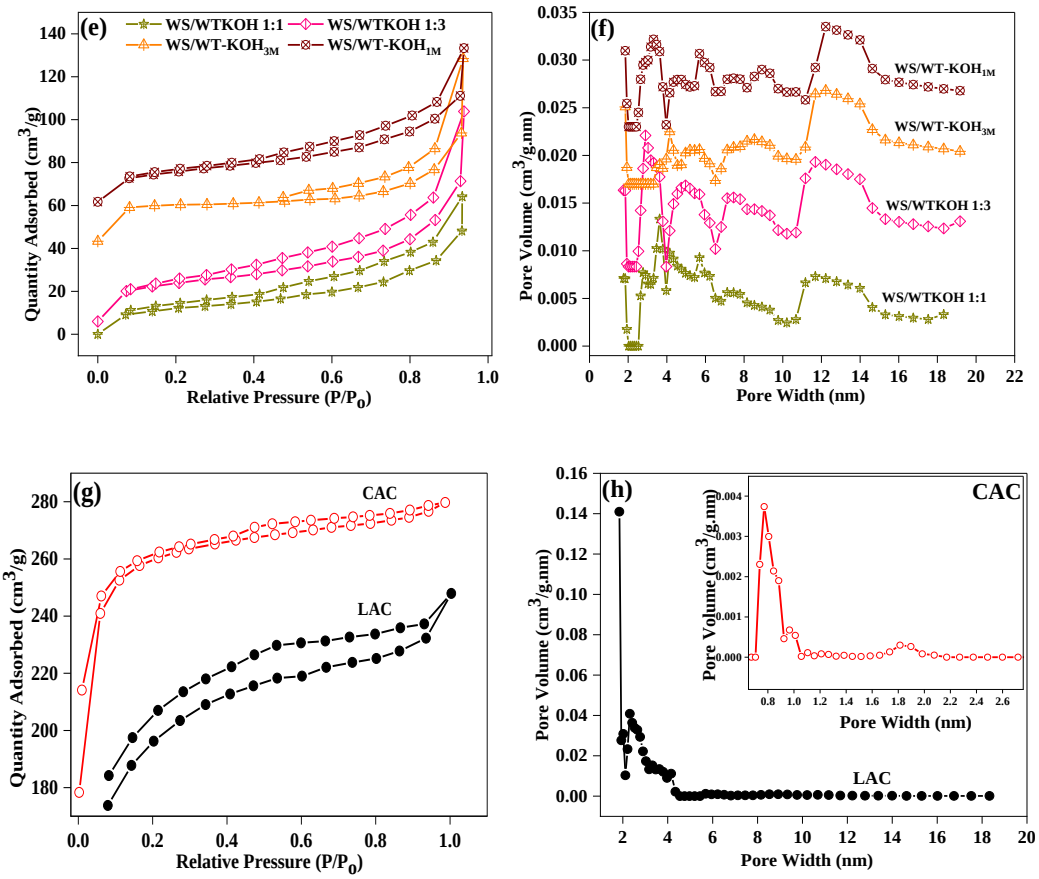

Figure 5: Nitrogen adsorption-desorption isotherms of activated samples (a) WSBC (c) WTBC (e) (WS/WT)BC (g) CAC and LAC and Pore size distribution of activated samples (b) WSBC (d) WTBC (f) (WS/WT)BC (h) CAC and LAC.

4.1.4 SEM-EDS Analysis

The morphologies of pristine and activated biochar were examined using scanning electron microscopy. Elements present on the surface of these biochar were also examined using EDS. The pristine BC exhibited aggregated morphology with some irregularly distributed pores. After KOH activation at 700°C, the WSKOH 1:3 presented well-developed porous structure Fig. 6(b) which increased the specific surface area and provide abundant active sites for adsorption of Cr (VI). Similar observations have been reported by He et al. 2019 (He et al., 2019). SEM of CAC and LAC were also performed for comparison and results revealed visibly smooth and flat structure with small pores on the surface of CAC whereas LAC has blocky structure (Fig. 6c-d). After Cr (VI) uptake, small particles were observed on the surface of WSKOH 1:3 as depicted from Fig. 6(e). These observations have been in line with the results of EDS where Cr(VI) anchored on the surface of WSKOH 1:3 (Table 4b).

Other common elements include C and O whereas trace elements of Si and N are also present.

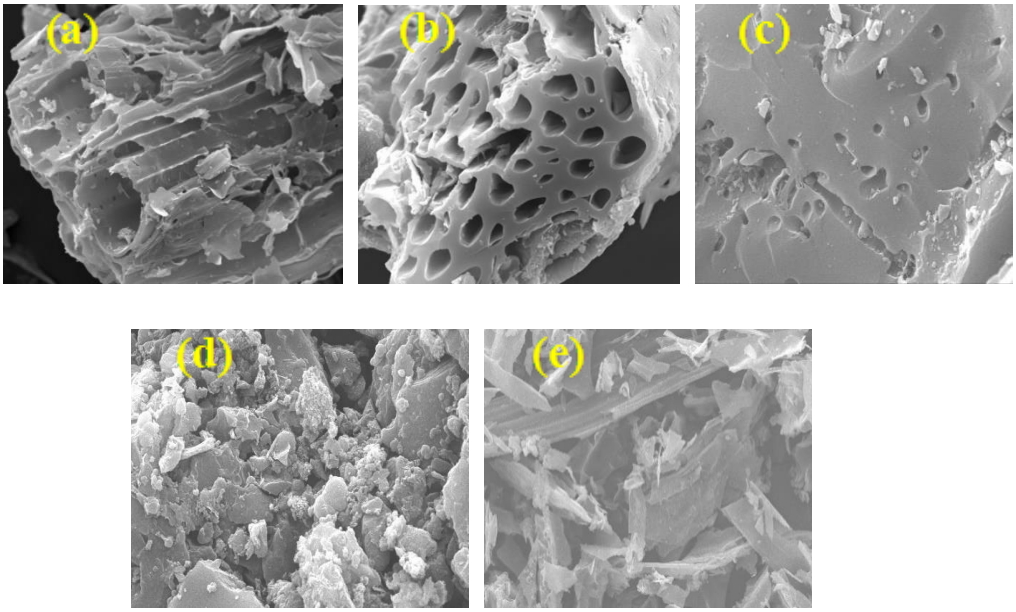

Figure 6: SEM images of raw and AC samples before and after Cr (VI) removal (a) WSBC (b) WSKOH 1:3 (c) CAC (d) LAC (e) WSKOH 1:3 after Cr(VI) uptake

Table 4: EDS of WSKOH 1:3 (a) before and (b) after Cr(VI) adsorption

(a)

Elements	Weight (%)	Atomic (%)	Error (%)
C	71.2	79.8	10.2
O	21.2	17.8	13.2
Si	2.4	1.2	6.1
K	0.8	0.3	10.7
Fe	1.3	0.3	13.8
Zn	3.1	0.6	5.1

(b)

Elements	Weight (%)	Atomic (%)	Error (%)
C	62.1	71.6	12.9
O	24.7	21.4	17.8
Si	3.8	1.9	10.6
K	0.9	0.3	26.5
N	3.5	3.5	100
Cr	4.9	1.3	12.8

4.1.5 FTIR Analysis

The FTIR spectra reflects the surface functional groups of WSBC, WTBC, WS/WT(BC) and the prepared AC (Fig. 7). The peaks in the range of 3450 cm^{-1} - 3200 cm^{-1} correspond to the −OH stretching vibrations of hydroxyl group (H. Zhang et al., 2020). Similarly, the peaks around 1750 – 1540 cm^{-1} correspond to the carboxylic group (C=O) and peaks at 1600 – 1450 cm^{-1} attributed to the aromatic C=C group (Shahrokhi-Shahraki et al., 2021). After activation, the strength of the peaks for all AC samples enhanced significantly as compared to their respective biochar samples, indicating that KOH activation is favorable for increasing surface functional groups of biochar (Yueyue Shi et al., 2020). The bands at 2923 cm^{-1} and 2913 cm^{-1} for WSBC and (WS/WT)BC and prepared AC samples represent C-H stretch of alkane group (M. Azharul Islam et al., 2015) (Fig 7a,c). The peaks around 1047 cm^{-1} for WS samples, 1020 cm^{-1} for WS/WT samples and 1013 cm^{-1} for WT samples represent C-O stretching in alcohols, and phenols (Kołodyńska et al., 2017). CAC, and LAC were also analyzed for FTIR spectrum and present peaks at 3440 cm^{-1}, 2921 cm^{-1}, 1630 cm^{-1} and 1068 cm^{-1} corresponded to −OH, C−H stretch of alkanes, C=O, and C− O stretch respectively (Fig 7d). After KOH modification, the rich oxygen containing functional groups such as -COOH, -OH, and -OCH3 gets positively charged in the acidic environment and attract the negatively charged Cr(VI) ions like $HCrO_4^-$and $Cr_2O_7^{2-}$ (X. Zhang et al., 2018). Moreover, the peak value of 2335 cm^{-1} for WSKOH 1:3, CAC and LAC related to CO_2 absorption (Shan et al., 2020). After adsorption of Cr (VI), the peaks of WSKOH 1:3 are either shifted to a new position or become weaker as depicted from Fig. 7d which might be due to the formation of complex between functional groups and Cr (Hotová et al., 2020).

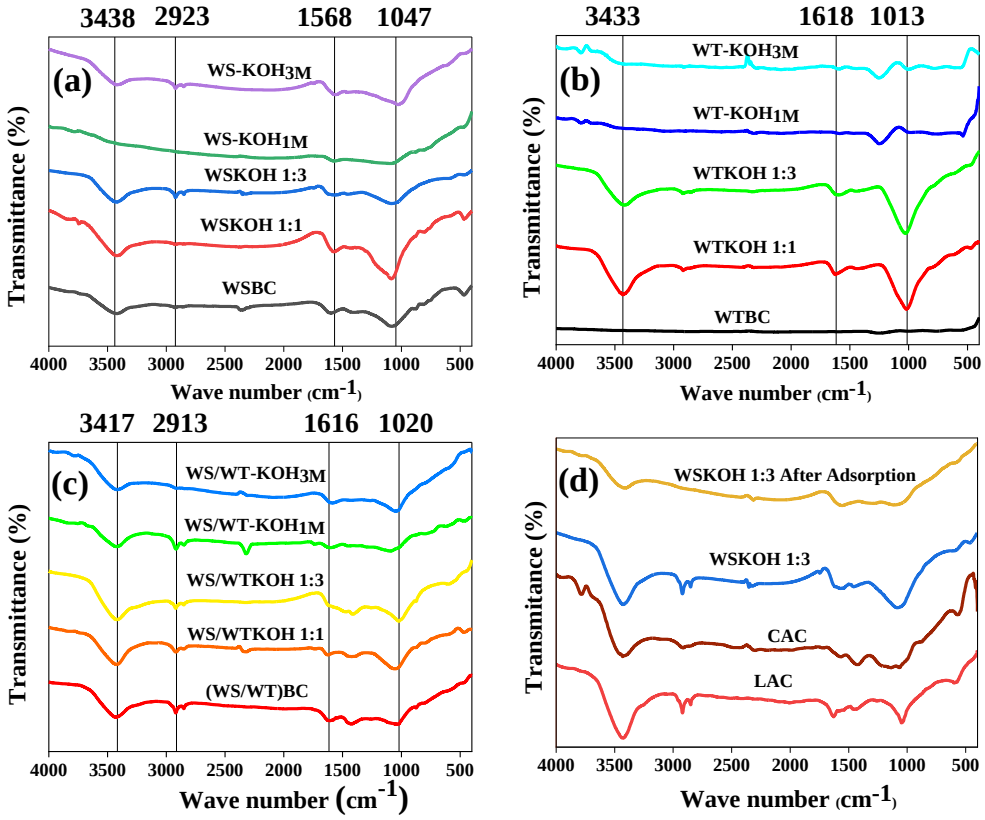

Figure 7: The FTIR spectrum of raw and activated samples (a) WSBC (b) WTBC (c) (WS/WT)BC (d) CAC, LAC, and WSKOH 1:3 after adsorption.

4.1.6 XRD Analysis

The XRD analysis was performed to investigate the crystallite morphology of the adsorbents. The XRD patterns of raw biochar and the samples prepared with dry activation method obtained in the 2θ range of 10° to 80° are presented in Fig. 8. It can be seen from Fig. 8(a,b,c) that all the samples present two broad peaks around 2θ = 20° – 25° and 41° – 43° correspond to the (002) and (100) crystal planes which reflect the typical peaks of amorphous carbon with non-crystalline structures (Qiu et al., 2019). The CAC and LAC also present broad peaks at 2θ = 23.85° and 43.23° (Fig.8d) which represent their amorphous nature. Moreover, the diffraction peaks of WSBC at 2θ = 28.03° and 40.35° are assigned to (200) and (220) crystal plans and of (WS/WT)BC at 2θ = 19.93°, 39.95°, and 56,65° correspond to the crystal planes of (020), (213), and (244) respectively which agree well with the database of KCl according to the JCPS card no. (41-1476) (Y. Wang et al., 2017). Similarly, the diffraction peaks at 2θ = 29.4° and 47.6° correspond to the crystal planes of (122) and (311) which agree well with amorphous structure of SiO_2 (JCPS card no. 01–089-

8936) (Y. Xu et al., 2021). After KOH activation, the KCl peak disappear as shown in Fig. 8(a,c), the reason for the disappearance of KCl could be due the thermal reaction between KCl and BC (J. Xu et al., 2022).

The crystallinity of raw biochar samples i.e., WSBC, WTBC, and (WS/WT)BC was 30.06%, 31.08%, and 30.84% respectively. After KOH activation, the crystallinity of the samples i.e., WSKOH 1:3, WTKOH 1:3, and WS/WTKOH 1:3 reduced to 28.28%, 24.85%, and 23.92% respectively as compared to raw samples. The decrease in crystallinity of AC samples indicate that the crystal structure of these samples damaged after alkali treatment due to which the stability of the structure changed (W. Wang et al., 2019). This have led to increase the porosity of theses samples that ultimately increased the adsorption capacity (K. Li et al., 2022). The crystallinity of CAC and LAC is 17.6% and 21.98% respectively. These results are consistent with SEM and BET analysis.

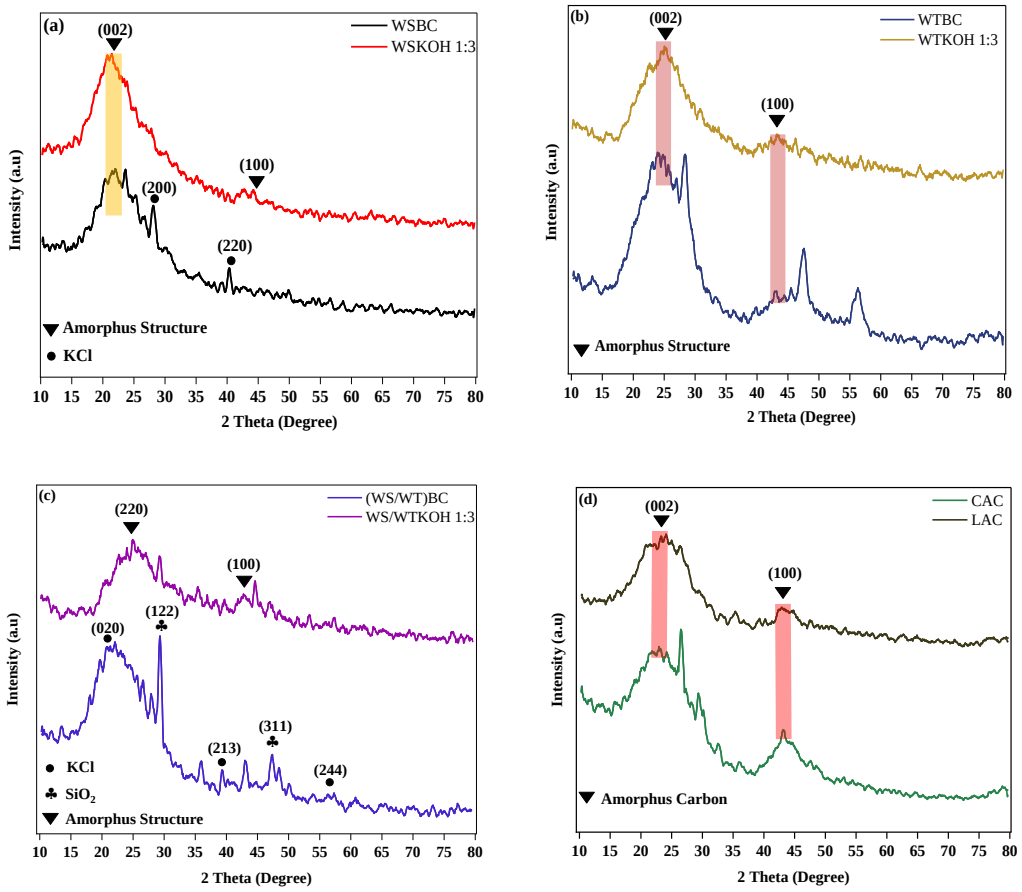

Figure 8: XRD patterns of raw and AC samples (a) WSBC and WSKOH 1:3 (b) WTBC and WTKOH 1:3 (c) (WS/WT)BC and WS/WTKOH 1:3 and (d) CAC and LAC.

4.1.7 Point of zero charge (PZC)

The point of zero charge (PZC) is the pH of solution where net surface charge is zero. The pristine biochar present neutral to slight basic PZC for WS (7.74 ± 0.02), WT (8.36 ± 0.02) and WS/WT (7.33 ± 0.02) respectively (Fig. 9a,b,c). Higher PZC for these samples indicate that basic groups dominate on the surface of these biochar (Herath et al., 2021). After activation, the PZC of WSKOH 1:3 (Fig. 9d) decreased to 4.87 ± 0.02. The washing process removed some of the ash content, hence decrease the PZC for WSKOH 1:3. Similar findings were also reported by (Dias et al., 2020). In a solution, pH below 4.87± 0.02 the surface of WSKOH 1:3 is positively charged and attract anionic ions. At solution pH above 4.87 ± 0.02 surface gets negatively charged and attract cations. Figure 9(e,f) illustrated that commercial activated samples (CAC and LAC) present similar PZC values to each other (6.71 ±0.02 and 6.85±0.02).

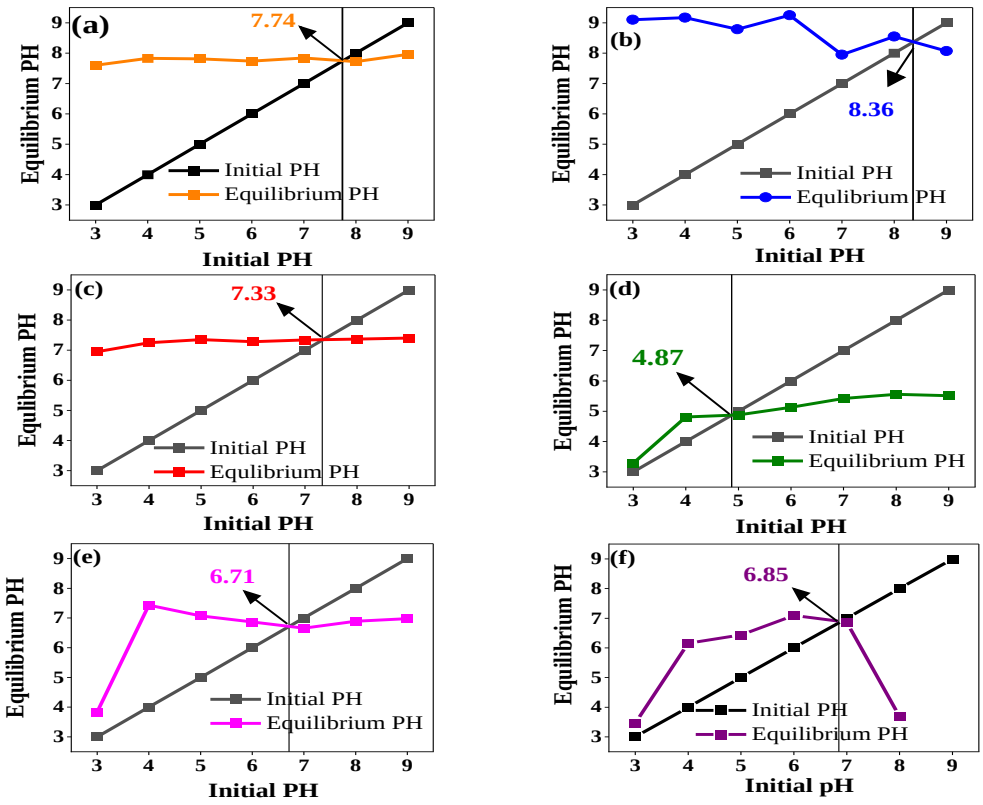

Figure 9: Point of zero charge (a) WSBC (b) WTBC (c) (WS/WT)BC (d) WSKOH 1:3 (e) CAC (f) LAC.

4.2 Activation Mechanism

The logical mechanism for the porous structure of biochar after KOH activated pyrolysis process was listed as follows (Y. T. Li et al., 2015).

$$6KOH + 2C \longrightarrow 2K + 2K_2CO_3 + 3H_2 \quad (11)$$

$$K_2CO_3 + C \longrightarrow K_2O + 2CO \quad (12)$$

$$K_2O + C \longrightarrow 2K + CO \quad (13)$$

$$K_2CO_3 \longrightarrow K_2O + CO_2 \quad (14)$$

$$2K + CO_2 \longrightarrow K_2O + CO \quad (15)$$

With increasing pyrolysis temperature, KOH began to form crystals, while thermal polymerization and curing activity on biochar began concurrently (Dai et al., 2019). As a result, biochar was compelled to form a porous sphere structure with KOH crystals inserted and become fixed in the pores. By further increasing the pyrolysis temperature, crystal KOH particles vaporize, and react with biochar, and the

subsequent potassium compounds like K_2CO_3, K_2O, and K further ruptured the biochar, exacerbating it to enlarge its surface area and inevitably replace the existing mesopores and macropores with new micropores. Diffusion of CO_2, CO and other gases produced more micropores on the surface of activated carbon.

4.3 Adsorption Results

In this section, adsorption results of Cr (VI) are presented.

4.3.1 Cr(VI) Standard curve

Diphenyl carbazide (DPC) standard method APHA 3500-CR was used for the detection of Cr (VI) using UV spectrophotometer. A red violet color indicates the presence of Cr (VI) ions in the solution. A calibration curve was prepared at λmax 540 nm using concentrations of Cr (VI) from 0.1 mg/L to 0.5 mg/L. Fig. 10 showed the calibration curve and the equation with a correlation factor R^2 0.9993.

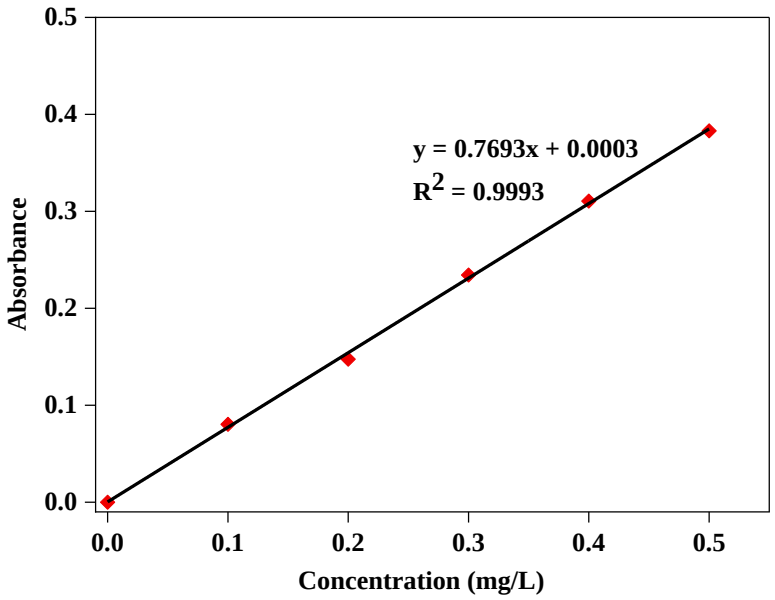

Figure 10: Standard curve of Chromium (VI)

4.3.2 Selection of Efficient Adsorbent

To evaluate the appropriate adsorbent for Cr (VI) adsorption, different adsorbents based on different activation methods including wet and dry activation were employed. The efficacy of these adsorbents was assessed based on Cr (VI) removal experiments. Figure 11 reveal the removal efficiency of different adsorbents. The removal efficiencies of WSBC, WTBC, and (WS/WT)BC are 16.29%, 35.39% and 29.28%, respectively. Less removal efficiency in case of raw biochar could be due the

poor surface properties as can be seen from Table 3. After wet activation, Cr VI) removal efficiency of WSBC increased with an increase in KOH concentration as shown in Fig.11. Similar trend was also observed for (WS/WT)BC. The reason for that could be the removal of organic debris present in the raw bio char (WSBC, (WS/WT)BC) after activation with KOH as reflected from the increased specific surface area (Table 3) similar findings was also reported by (X. Zhang et al., 2018). whereas in case of WTBC, removal efficiency tends to decrease with an increase in the concentration of KOH.

In case of dry activation, the removal efficiency increased by increasing the KOH impregnation ratio (1:1, 1:3) for WSBC and (WS/WT)BC. In comparison to wet activation method, the removal efficiency is much higher in dry activation method and is well explained from the polarity of the adsorbents, BET, FTIR, and XRD results. The adsorbent (WSKOH 1:3) showed the maximum Cr (VI) removal efficiency of 99.56%. The better results for WSKOH 1:3 could be due to the huge increase in its surface area (529.481 m^2/g). WTBC showed the similar trend of decreasing removal efficiency with the increase of biochar to KOH ratio. Based on the results of characterization phase and removal results, the WSKOH 1:3 adsorbent from dry activation method was selected for further experimentation.

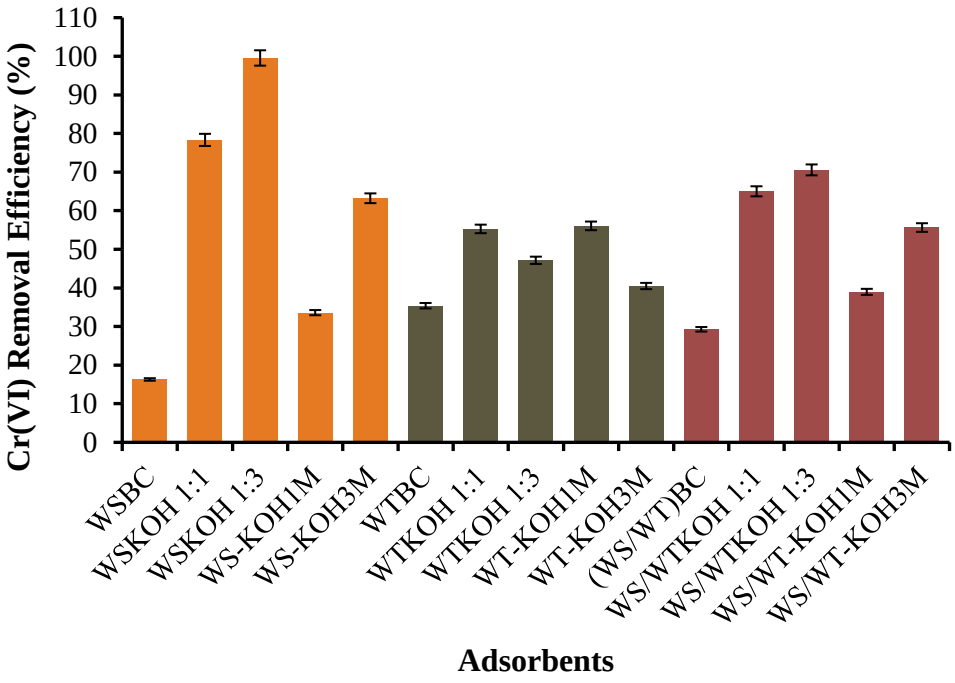

Figure 11: Types of Adsorbents used for removal of Cr (VI). Experimental conditions: Co = 20 mg/L; Adsorbent dosage = 1 g/L; pH = 2; Contact time = 120 mins.

4.3.3 Effect of Adsorbent dosage

Adsorbent dose is a critical constraint influencing the adsorption capacity of an adsorbent under given adsorbate concentration and operating conditions. Figure 12 represents the removal efficiency and adsorption capacity of Cr (VI) on WSKOH 1:3 at different doses (0.5, 1, 2, 3, 5, 7 g). As the adsorbent dose increased removal efficiency also increases whereas adsorption capacity reduced. This increment was assigned to more active sites and large surface area for high adsorbent doses (Panda et al., 2017). It was noticed that removal efficiency increased rapidly when the adsorbent dose increased from 0.5 g to 2 gL^{-1} as compared to 2 to 7 gL^{-1}. In comparison adsorption capacity tends to decrease with an increase in adsorbent dose. This trend was attributed to the fact that for a particular initial concentration of adsorbate available sites and surface area was larger and the intensity of adsorbate loaded onto the unit surface area was lower (Y. Zhao et al., 2013).

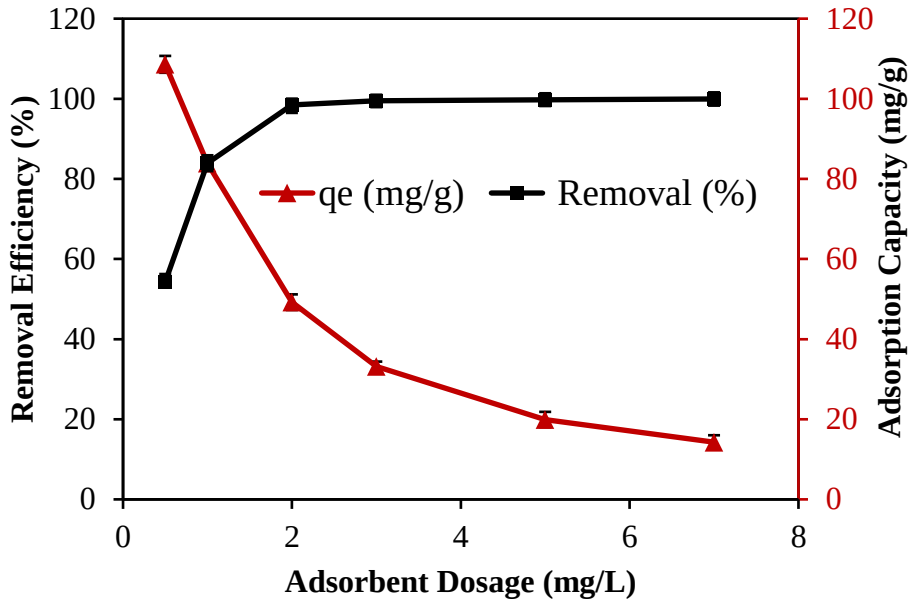

Figure 12: Effect of adsorbent dosage on Cr (VI) removal efficiency and uptake onto WSKOH 1:3. Experimental conditions: Co = 100 mg/L; Contact Time = 120 mins; pH = 2

4.3.4 Effect of pH

During adsorption process, solution pH can substantially influence ionization degree of adsorbate and functional groups on the surface of adsorbent (J. Li et al., 2017). It is well established that Cr (VI) exists as soluble species $HCrO_4^-$, $Cr_2O_7^{2-}$ at PH <6 and CrO_4^{2-} at PH > 7 (Qu et al., 2021). As depicted from Fig. 13 removal of Cr (VI) greatly depends on the solution pH. At pH 2.0 the removal efficiency was 98.47% which then reduced to 39.66% as the pH value went up to 9.0. PZC of WSKOH 1:3 was 4.87 as shown in (Fig. 9d) point out that adsorbent is positively charged when $pH_{solution}$ is less than 4.87 and exhibits electronegativity at pH above 4.87. When $pH_{solution}$ < PZC the surface charge of the adsorbent gets protonated and contributes for the uptake of negatively charged $HCrO_4^-$, $Cr_2O_7^{2-}$ due to electrostatic attraction (Qu et al., 2019). However, Cr (VI) uptake declined exceptionally at high pH values due the electrostatic repulsive effect (Hu et al., 2020). Thus, contemplating the removal efficiency and chemical addition for pH adjustment, PH 2.0 was considered as optimum value for Cr (VI) adsorption.

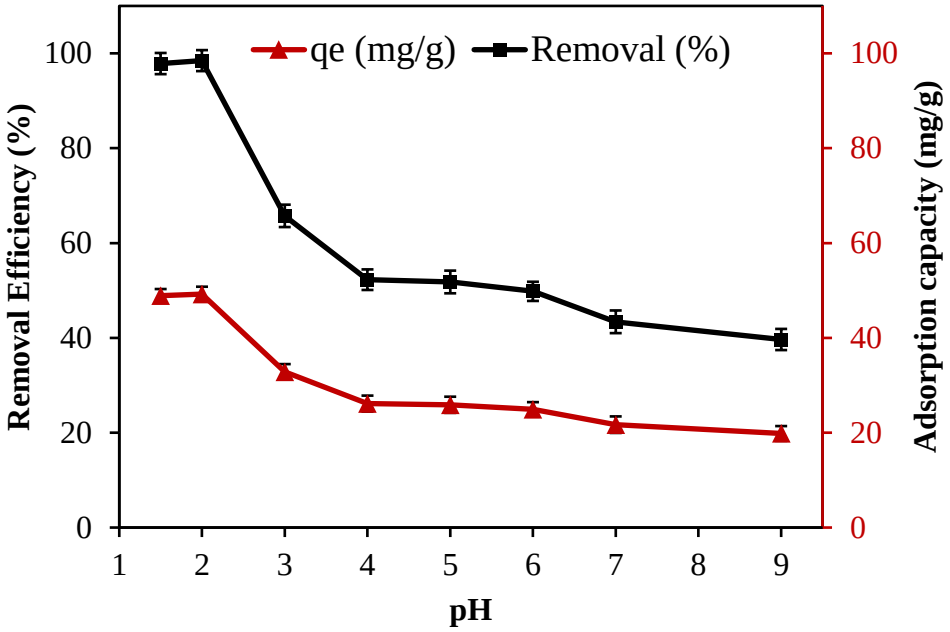

Figure 13: Effect of pH on Cr (VI) removal efficiency and uptake of Cr (VI) onto WSKOH 1:3. Experimental conditions: Co = 100mg/L; adsorbent dosage = 2 g/L; time = 120 mins.

4.3.5 Effect of Contact time

To explore the adsorptive rate of Cr (VI), time reliant experiments were conducted. It can be seen from Fig. 14 that removal efficiency of WSKOH 1:3 increased quickly removing more than 80% of Cr (VI) from solution during first 60 minutes. High adsorption removal rates during first 60 minutes reveals large no. of active sites are available (Y. Ma et al., 2021). With more rise in the contact time the adsorption process decelerated and reached equilibrium after 120 minutes for WSKOH 1:3. Thus, further increase in contact time did not have any significant effect (Pellera et al., 2012) and 120 minutes were considered as equilibrium time for Cr (VI) removal.

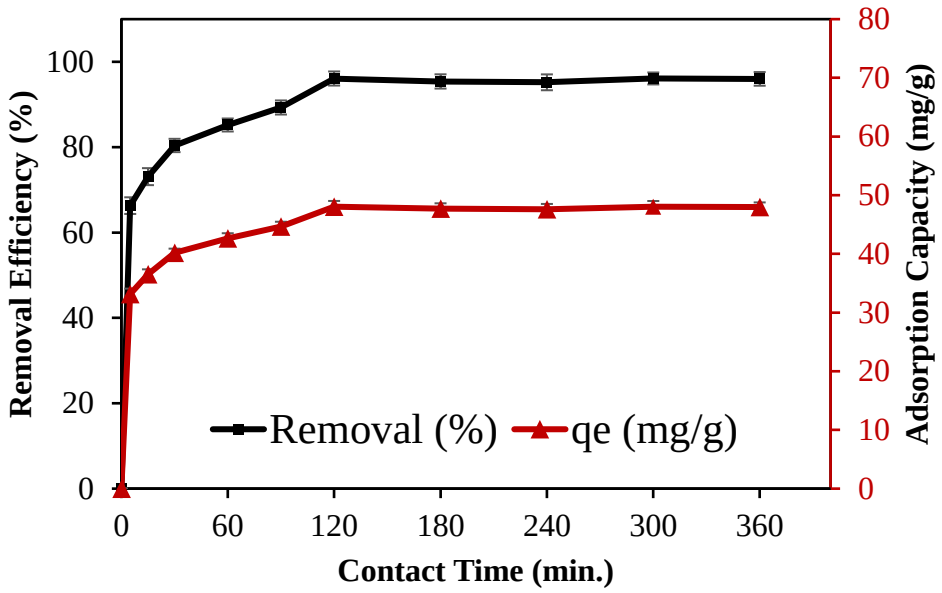

Figure 14: Effect of contact time on Cr (VI) removal efficiency and uptake of Cr(VI) onto WSKOH 1:3. Experimental conditions: Co = 100 mg/L; adsorbent dosage = 2 g/L; PH = 2.

4.3.6 Effect of Cr (VI) Initial concentration

The influence of several initial concentrations of Cr (VI) on adsorption capacity is shown in Fig. 15. It can be seen from figure that adsorption capacity increased from 4.96 mg/g to 101.39 mg/g while removal efficiency(%) decreased from 99.35% to 81.11% with an increase in initial concentration of Cr (VI) from 10 mg/L to 250 mg/L. This increase in adsorption capacity results from higher pollutant i.e., Cr (VI) concentration, which offer higher driving force to overcome all mass transfer resistances, that ultimately result in high Cr (VI) adsorption (M. Azharul Islam et al., 2015);(Kumar & Jena, 2017).

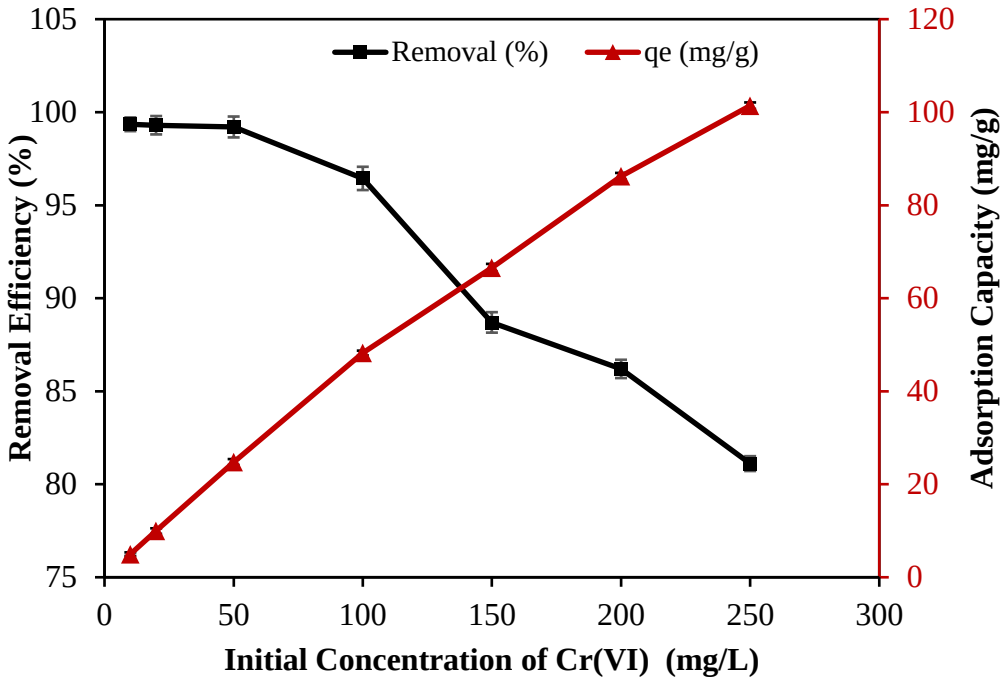

Figure 15: Effect of Initial concentration on Cr (VI) removal efficiency and uptake of Cr (VI) onto WSKOH 1:3. Experimental conditions: Adsorbent dosage = 2 g/L; PH = 2 contact time = 120 minutes.

4.4 Comparison with Commercial Activated Carbon

Two commercial Activated carbon CAC and LAC were also used for comparison purposes with WSKOH 1:3 to remove Cr (VI) at optimized conditions. The result showed that WSKOH 1:3 performed better with a removal efficiency of 98.47% as compared to 93.09% for CAC and 87.32% for LAC respectively. The results are shown in Fig. 16.

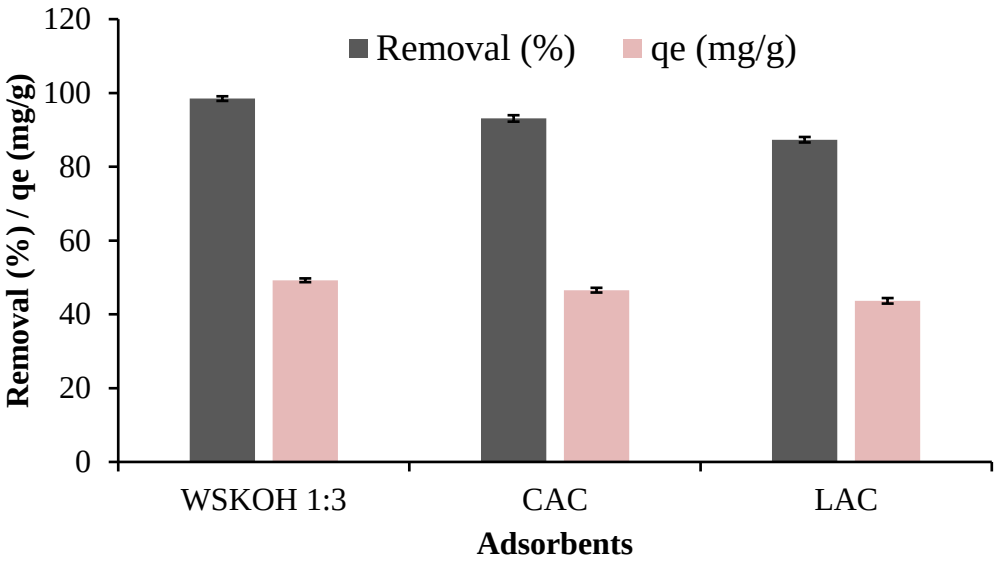

Figure 16: Comparison of WSKOH 1:3, CAC, and LAC. Experimental conditions: Initial Cr (VI) concentration = 100 mg/L, Adsorbent dosage = 2 g/L; PH = 2, contact time = 120 minutes.

4.5 Kinetic and Isotherm Studies

Adsorption of Cr (VI) was analyzed using the kinetic and isotherm studies.

4.5.1 Adsorption kinetics

To quantitatively evaluate the adsorption kinetics and mechanism for adsorption the experimental data of WSKOH 1:3 was fitted by pseudo first order, and pseudo second order kinetic models. The fitted plots are shown in Fig. 17. Adsorption process of WSKOH 1:3 was better fitted with pseudo second order kinetic model with correlation coefficient R^2 of 0.98 as compared to the pseudo first order (R^2= 0.93) for WSKOH 1:3. The calculated values of adsorption capacity (mg/g) were close to the experimental values as depicted from Table 5. Therefore, these results proposed the adsorption of Cr (VI) onto the porous adsorbent was subjugated by chemisorption by sharing or exchanging of electrons between adsorbents and Cr (VI) (Shan et al., 2020).

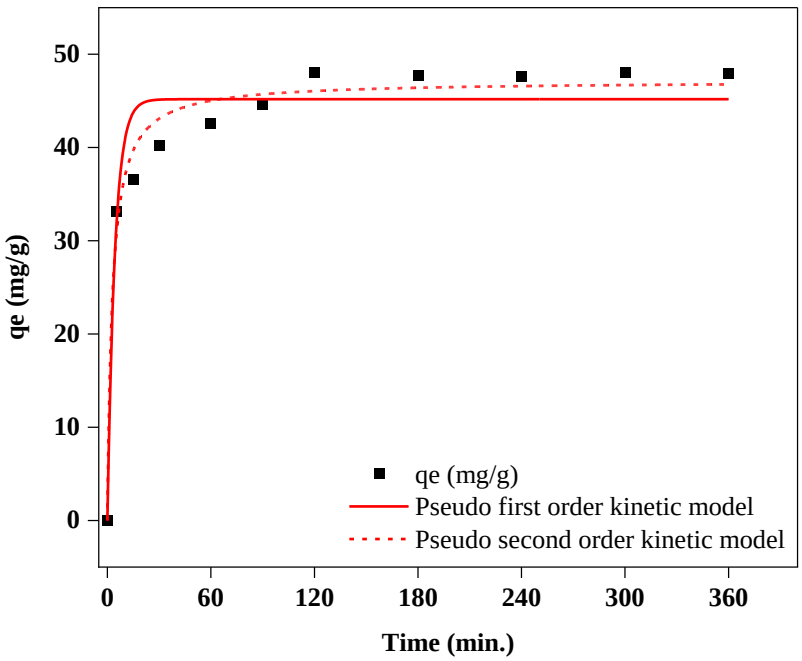

Figure 17: Adsorption kinetics fitted plots of WSKOH 1:3.

Table 5: Kinetic model Parameters for adsorption of Cr (VI).

		Pseudo-first order Model			Pseudo-second order Model		
Adsorbent	q_e, exp. (mg/g)	q_e, cal. (mg/g)	K_1 (min^{-1})	R^2	q_e, cal. (mg/g)	K_2 (g mg^{-1} min^{-1})	R^2
WSKOH 1:3	48.04	45.17	0.23	0.93	47.13	0.0075	0.98

q_e, exp. – q_e, experimental; q_e, cal. – q_e, calculated

4.5.2 Adsorption Isotherms

The Langmuir and Freundlich isotherm models were used to quantitatively analyze the adsorption performance of Cr (VI) by WSKOH 1:3 (Fig 18). Data were fitted by nonlinear regression using Origin Pro 2021 Software. Results presented in Table 7 have shown that Freundlich isotherm model better describe the adsorption of Cr (VI) by WSKOH 1:3 with a higher correlation coefficient of (0.981, 0.966, 0.990) as compared to Langmuir isotherm model (0.935, 0.941, 0.943) under each temperature. Freundlich isotherm suggested that the uptake of Cr (VI) occurred on the multifaceted surface of adsorbent, succeeding in multilayer adsorption on the surface

of binding sites between surface functional groups of WSKOH 1:3 and Cr (VI) (N. Zhao et al., 2017b) . The $1/n_F$ value of Freundlich isotherm model was less than 1 and proposed that the adsorption of Cr (VI) onto the WSKOH 1:3 was favored by chemical adsorption (Yueyue Shi et al., 2020). Moreover, the maximum Langmuir uptake(q_{max}) of WSKOH 1:3 for Cr (VI) was estimated to be 96.08 mg/g at 25°C which is comparable to other adsorbents previously reported as shown in Table 6.

Table 6: Summary of different activated carbons for Cr (VI) uptake.

Raw material	Activating Agent	S_{BET} (m^2/g)	Adsorption capacity of Cr(VI)(mg/g)	pH	References
Waste Tire	H_3PO_4	4.07	102.90	2.0	(Sivaraman et al., 2022)
Corn Stalk	KOH	498	89.5	4.5	(J. Zhao et al., 2020b)
Apple peels	H_3PO_4	-	36.01	2.0	(Enniya et al., 2018)
Eucalyptus camaldulensis sawdust	H_3PO_4	217.14	104	3.0	(Haroon et al., 2020)
Mixed waste tea	-	13.86	94.34	2.0	(Cherdchoo et al., 2019)
Wheat straw	KOH	529.48	96.08	2.0	This study

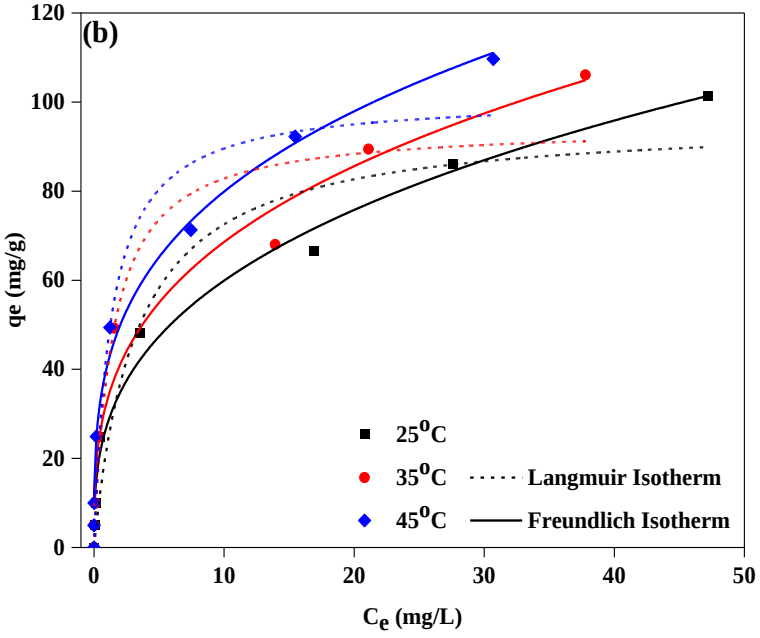

Figure 18: Adsorption Isotherms of WSKOH 1:3.

Table 7: Adsorption Isotherm parameters

		Langmuir parameters			Freundlich parameters		
Adsorbent	T (°C)	q_{max} (mg/g)	K_L (L/mg)	R^2	$1/n_F$	k_F (mg/g)(L/mg)$^{1/n}$	R^2
WSKOH 1:3	25	96.082	0.314	0.935	0.339	27.441	0.98
	35	97.657	0.700	0.941	0.319	32.838	0.96
	45	101.109	0.776	0.943	0.293	40.619	0.99

4.6 Thermodynamic parameters

Thermodynamic analysis was performed to understand the mechanism involved in the adsorption of Cr (VI) onto the adsorbent (WSKOH 1:3). The thermodynamic parameters (ΔG°, ΔH°, ΔS°) was investigated in the temperature range of 25°C to 45°C. Results are tabulated in Table 8. The negative values of ΔG for WSKOH 1:3 at all temperatures indicate that the adsorption process is impulsive (Fan & Zhang, 2018). However, the absolute value of ΔG increases with the increase in temperature, suggesting that increase in temperature favors the spontaneous reaction (H. Ma et al.,

2019). The positive value of ΔH for Cr(VI) uptake indicates that Cr(VI) capture by WSKOH 1:3 was an endothermic process (M. J. Ahmed et al., 2019). The adsorption type can be split into physical adsorption (2.1–20.9 kJ/mol) and chemical adsorption (20.9–418.4 kJ/mol) based on the value of ΔH (C. Sun et al., 2012). Form Table 8, the value of ΔH is 35.89 kJ/mol indicating that adsorption of Cr (VI) by WSKOH 1:3 was chemical adsorption. These findings are consistent with isotherm studies. Furthermore, the positive value of ΔS indicates the increased randomness at the solid/liquid interface during the adsorption of Cr (VI) on WSKOH 1:3 (B. Chen et al., 2019).

Table 8: Thermodynamic parameters for Cr (VI) onto WSKOH 1:3

T (^oC)	ΔG° (KJ/mol)	ΔH° (KJ/mol)	$\Delta S°$ ($KJmol^{-1}k^{-1}$)
25	-14.249	35.89	0.1692
35	-16.777		
45	-17.596		

4.7 Regeneration Studies

The reusability of the adsorbent is an important factor in determining its practical application in industry (Xie et al., 2019) . Adsorption of Cr (VI) is highly dependent on pH of the solution and difficult to desorb with acidic reagents**.** Results of Cr (VI) adsorption-desorption are depicted in Fig. 19 and indicate that removal of Cr (VI) using regenerated WSKOH 1:3 maintained over 65% after first three cycles. While decreased to 48.98% after fourth cycle. Meanwhile the desorption efficiency was far less than that of adsorption. It decreased from 74.77% after first cycle to 26.795% after fourth cycle. Results concluded that strong chemosorption of Cr (VI) occur on the adsorbent surface (Guo et al., 2018). Decrease in adsorption-desorption efficiencies during each cycle could be due to the blockage of pores and hard desorption of complex between functional groups and Cr (VI), which ultimately reduce the active sites on the surface of adsorbent (Qu et al., 2021). Overall, results suggested WSKOH 1:3 to be dependable adsorbent and can be applied for practical application.

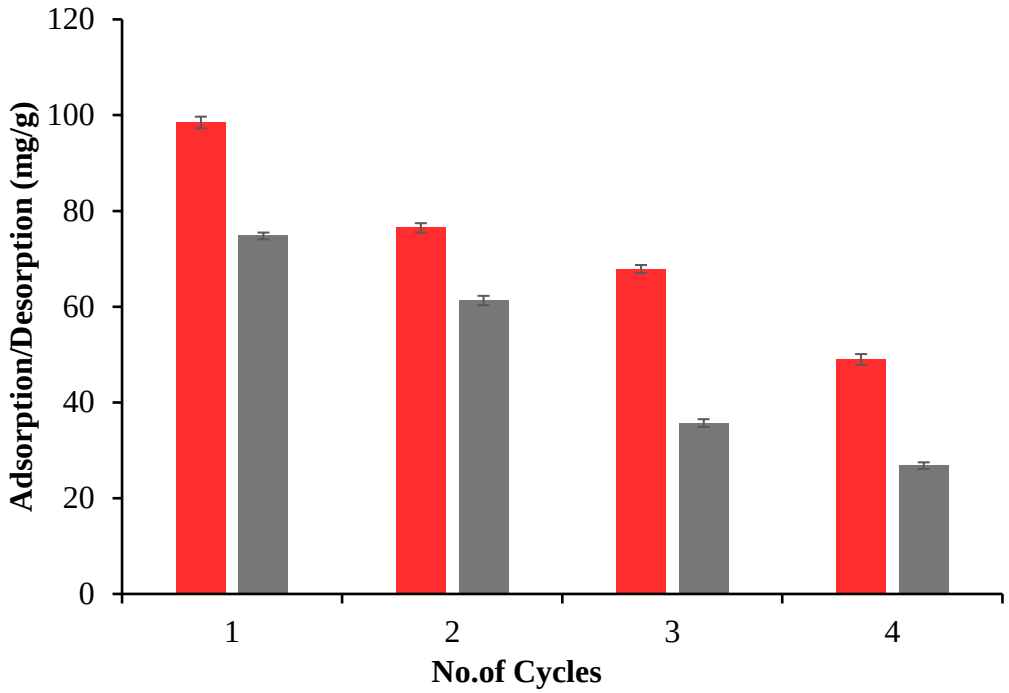

Figure 19: Regeneration performance of WSKOH 1:3. Experimental conditions: Co = 100mg/L; T = 25°C; Adsorbent dosage = 2g/L

4.8 Mechanism of Cr (VI) Adsorption

Adsorption experiments were performed to understand the mechanism involved for the removal of Chromium (VI). Removal of Chromium (VI) from aqueous solution depends on the pH of the solution. The maximum removal percentage achieved in this study was at pH 2 and was selected as optimum pH. In acidic conditions, the functional groups present on the surface of the adsorbent such as hydroxyl group (-OH), carboxyl group (COOH) get protonated and adsorb the negatively charged chromium species. Moreover, at pH < 3 the dominant form of chromium is $HCrO_4^-$ and require only singular site for adsorption whereas, at pH > 3 the dominant forms of chromium are $Cr_2O_7^{2-}$, CrO_4^{2-} which require at least two exchangeable sites for adsorption. This electrostatic phenomenon was well supported by the kinetic and isotherm studies where Pseudo second order (PSO) kinetic model and Freundlich Isotherm model better fit the experimental data revealing that the adsorption process is controlled through chemisorption. SEM of the adsorbent WSKOH 1:3 after uptake of Chromium (VI) had a blocky structure as shown in Fig. 6(b) which might be due to the uptake of Chromium (VI). This is also confirmed by

EDS results (Table 4a,b). Moreover, the FTIR curves of WSKOH 1:3 after uptake of Cr (VI) as shown in Fig. 7(d) clearly indicate a shift of the curve after binding of Cr. This could be due to the complexation (Eqs.(16) - (17)) between adsorbent active sites and Cr. Ion exchange (Eq.18) process was also involved in the adsorption process. Thus, overall mechanism of Cr(VI) adsorption onto WSKOH 1:3 involve chemical adsorption i.e., Ion exchange, electrostatic attraction, and complexation between functional groups on the surface of adsorbent and chromium.

$$R - COO^{-} + Cr^{6+} \longrightarrow R - COO^{-}\ldots.Cr^{6+} \quad (16)$$

$$R - O^{-} + Cr^{6+} \longrightarrow R - O^{-}\ldots.Cr^{6+} \quad (17)$$

$$R - COOH + Cr^{6+} \longrightarrow R - COO^{-}\ldots.Cr^{6+} + H^{+} \quad (18)$$

CHAPTER 5

Conclusion

5.1 Conclusion

In this study, different feedstocks (WS, WT, WS/WT) were employed to prepare biochar that was chemically activated by two different activation methods for the adsorption of Cr (VI). The results showed that WSKOH 1:3 prepared by dry activation, possessed larger specific surface area (529.48 m^2/g), more active sites, and well-developed porous structure as compared to other activated carbon samples prepared by both dry and wet activation methods. When pH value is 2, the removal efficiency of Cr (VI) from WSKOH 1:3 reached 98.47% which is higher than other prepared activated samples and commercial AC (CAC and LAC). The adsorption data better fitted the PSO kinetic model and Freundlich isotherm model. The thermodynamic studies showed that adsorption of Cr (VI) onto WSKOH 1:3 was spontaneous and endothermic in nature. Further investigation into Cr (VI) removal revealed that electrostatic attraction, ion exchange, complexation of cr species with WSKOH 1:3, and reduction of Cr (VI) to Cr (III) are the primary mechanisms of Cr (VI) binding on the surface of WSKOH 1:3. Overall, the WSKOH 1:3 proved to be a promising adsorbent for the removal Cr (VI) from water.

References

Abbaci, F., Nait-Merzoug, A., Guellati, O., Harat, A., el Haskouri, J., Delhalle, J., Mekhalif, Z. & Guerioune, M. (2022). Bio/KOH ratio effect on activated biochar and their dye based wastewater depollution. *Journal of Analytical and Applied Pyrolysis*, *162*(January), 105452. https://doi.org/10.1016/j.jaap.2022.105452

Acosta, R., Fierro, V., Martinez de Yuso, A., Nabarlatz, D. & Celzard, A. (2016). Tetracycline adsorption onto activated carbons produced by KOH activation of tyre pyrolysis char. *Chemosphere*, *149*, 168–176. https://doi.org/10.1016/j.chemosphere.2016.01.093

Adam, M. R., Salleh, N. M., Othman, M. H. D., Matsuura, T., Ali, M. H., Puteh, M. H., Ismail, A. F., Rahman, M. A. & Jaafar, J. (2018). The adsorptive removal of chromium (VI) in aqueous solution by novel natural zeolite based hollow fibre ceramic membrane. *Journal of Environmental Management*, *224*(July), 252–262. https://doi.org/10.1016/j.jenvman.2018.07.043

Aghababaei, A., Ncibi, M. C. & Sillanpää, M. (2017). Optimized removal of oxytetracycline and cadmium from contaminated waters using chemically-activated and pyrolyzed biochars from forest and wood-processing residues. *Bioresource Technology*, *239*, 28–36. https://doi.org/10.1016/j.biortech.2017.04.119

Agrafioti, E., Kalderis, D. & Diamadopoulos, E. (2014). Arsenic and chromium removal from water using biochars derived from rice husk, organic solid wastes and sewage sludge. *Journal of Environmental Management*, *133*, 309–314. https://doi.org/10.1016/j.jenvman.2013.12.007

Ahmed, M. B., Zhou, J. L., Ngo, H. H., Guo, W. & Chen, M. (2016). Progress in the preparation and application of modified biochar for improved contaminant removal from water and wastewater. *Bioresource Technology*, *214*, 836–851. https://doi.org/10.1016/j.biortech.2016.05.057

Ahmed, M. J., Okoye, P. U., Hummadi, E. H. & Hameed, B. H. (2019). High-performance porous biochar from the pyrolysis of natural and renewable seaweed (Gelidiella acerosa) and its application for the adsorption of methylene blue. *Bioresource Technology*, *278*(January), 159–164. https://doi.org/10.1016/j.biortech.2019.01.054

Ai, T., Jiang, X., Liu, Q., Lv, L. & Wu, H. (2019). Daptomycin adsorption on magnetic ultra-fine wood-based biochars from water: Kinetics, isotherms, and mechanism studies. *Bioresource Technology*, *273*(September 2018), 8–15. https://doi.org/10.1016/j.biortech.2018.10.039

Alshameri, A., He, H., Zhu, J., Xi, Y., Zhu, R., Ma, L. & Tao, Q. (2018). Adsorption of ammonium by different natural clay minerals: Characterization, kinetics and adsorption isotherms. *Applied Clay Science*, *159Alshame*(November 2017), 83–93. https://doi.org/10.1016/j.clay.2017.11.007

Amen, R., Yaseen, M., Mukhtar, A., Klemeš, J. J., Saqib, S., Ullah, S., Al-Sehemi, A. G., Rafiq, S., Babar, M., Fatt, C. L., Ibrahim, M., Asif, S., Qureshi, K. S., Akbar, M. M. & Bokhari, A. (2020). Lead and cadmium removal from wastewater using eco-friendly biochar adsorbent derived from rice husk, wheat straw, and corncob. *Cleaner Engineering and Technology*, *1*(October), 100006. https://doi.org/10.1016/j.clet.2020.100006

Babu, A. R., Yusub, S., Teja, P. M. V., Rao, P. S., Aruna, V. & Rao, D. K. (2019). Effect of Cr2O3 on the structural, optical and dielectric studies of LiF-SrO-B2O3 glasses. *Journal of Non-Crystalline Solids*, *520*(February), 119428. https://doi.org/10.1016/j.jnoncrysol.2019.05.004

Basumatary, A. K., Kumar, R. V., Ghoshal, A. K. & Pugazhenthi, G. (2016). Cross flow ultrafiltration of Cr (VI) using MCM-41, MCM-48 and Faujasite (FAU) zeolite-ceramic composite membranes. *Chemosphere*, *153*, 436–446. https://doi.org/10.1016/j.chemosphere.2016.03.077

Bhatnagar, A. & Minocha, A. K. (2006). Conventional and non-conventional adsorbents for removal of pollutants from water - A review. *Indian Journal of Chemical Technology*, *13*(3), 203–217.

Bohdziewicz, J. (2000). Removal of chromium ions (VI) from underground water in the hybrid complexation-ultrafiltration process. *Desalination*, *129*(3), 227–235. https://doi.org/10.1016/S0011-9164(00)00063-1

Chen, B., Chen, S., Zhao, H., Liu, Y., Long, F. & Pan, X. (2019). A versatile B-cyclodextrin and polyethyleneimine bi-functionalized magnetic nanoadsorbent for simultaneous capture of methyl orange and Pb(II) from complex wastewater. *Chemosphere*, *216*, 605–616. https://doi.org/10.1016/j.chemosphere.2018.10.157

Chen, D., Cheng, Y., Zhou, N., Chen, P., Wang, Y., Li, K., Huo, S., Cheng, P., Peng, P., Zhang, R., Wang, L., Liu, H., Liu, Y. & Ruan, R. (2020). Photocatalytic degradation of organic pollutants using TiO2-based photocatalysts: A review. *Journal of Cleaner Production*, *268*, 121725. https://doi.org/10.1016/j.jclepro.2020.121725

Cherdchoo, W., Nithettham, S. & Charoenpanich, J. (2019). Removal of Cr(VI) from synthetic wastewater by adsorption onto coffee ground and mixed waste tea. *Chemosphere*, *221*, 758–767. https://doi.org/10.1016/j.chemosphere.2019.01.100

Costa, M. (2003). Potential hazards of hexavalent chromate in our drinking water. *Toxicology and Applied Pharmacology*, *188*(1), 1–5. https://doi.org/10.1016/S0041-008X(03)00011-5

Dai, X. H., Fan, H. X., Zhang, J. J. & Yuan, S. J. (2019). Sewage sludge-derived porous hollow carbon nanospheres as high-performance anode material for lithium ion batteries. *Electrochimica Acta*, *319*, 277–285. https://doi.org/10.1016/j.electacta.2019.07.006

Danish, M. & Ahmad, T. (2018). A review on utilization of wood biomass as a sustainable precursor for activated carbon production and application. *Renewable and Sustainable Energy Reviews*, *87*(February), 1–21. https://doi.org/10.1016/j.rser.2018.02.003

Das, C., Singh, S., Bhakta, S., Mishra, P. & Biswas, G. (2021). Bio-modified magnetic nanoparticles with Terminalia arjuna bark extract for the removal of

methylene blue and lead (II) from simulated wastewater. *Chemosphere*, *November*, 132673. https://doi.org/10.1016/j.chemosphere.2021.132673

di Stasi, C., Alvira, D., Greco, G., González, B. & Manyà, J. J. (2019). Physically activated wheat straw-derived biochar for biomass pyrolysis vapors upgrading with high resistance against coke deactivation. *Fuel*, *255*(April), 115807. https://doi.org/10.1016/j.fuel.2019.115807

Dias, D., Bernardo, M., Matos, I., Fonseca, I., Pinto, F. & Lapa, N. (2020). Activation of co-pyrolysis chars from rice wastes to improve the removal of Cr3+ from simulated and real industrial wastewaters. *Journal of Cleaner Production*, *267*. https://doi.org/10.1016/j.jclepro.2020.121993

Doke, S. M. & Yadav, G. D. (2014). Process efficacy and novelty of titania membrane prepared by polymeric sol-gel method in removal of chromium(VI) by surfactant enhanced microfiltration. *Chemical Engineering Journal*, *255*, 483–491. https://doi.org/10.1016/j.cej.2014.05.098

Duan, X. L., Yuan, C. G., Jing, T. T. & Yuan, X. D. (2019). Removal of elemental mercury using large surface area micro-porous corn cob activated carbon by zinc chloride activation. *Fuel*, *239*(November 2018), 830–840. https://doi.org/10.1016/j.fuel.2018.11.017

Elfeky, S. A., Mahmoud, S. E. & Youssef, A. F. (2017). Applications of CTAB modified magnetic nanoparticles for removal of chromium (VI) from contaminated water. *Journal of Advanced Research*, *8*(4), 435–443. https://doi.org/10.1016/j.jare.2017.06.002

Enniya, I., Rghioui, L. & Jourani, A. (2018). Adsorption of hexavalent chromium in aqueous solution on activated carbon prepared from apple peels. *Sustainable Chemistry and Pharmacy*, *7*(November 2017), 9–16. https://doi.org/10.1016/j.scp.2017.11.003

Fan, C. & Zhang, Y. (2018). Adsorption isotherms, kinetics and thermodynamics of nitrate and phosphate in binary systems on a novel adsorbent derived from corn stalks. *Journal of Geochemical Exploration*, *188*(January), 95–100. https://doi.org/10.1016/j.gexplo.2018.01.020

Farooq, M. Z., Zeeshan, M., Iqbal, S., Ahmed, N. & Shah, S. A. Y. (2018). Influence of waste tire addition on wheat straw pyrolysis yield and oil quality. *Energy*, *144*, 200–206. https://doi.org/10.1016/j.energy.2017.12.026

Farooqi, Z. H., Akram, M. W., Begum, R., Wu, W. & Irfan, A. (2021). Inorganic nanoparticles for reduction of hexavalent chromium: Physicochemical aspects. *Journal of Hazardous Materials*, *402*(July 2020), 123535. https://doi.org/10.1016/j.jhazmat.2020.123535

Fu, F., Ma, J., Xie, L., Tang, B., Han, W. & Lin, S. (2013). Chromium removal using resin supported nanoscale zero-valent iron. *Journal of Environmental Management*, *128*, 822–827. https://doi.org/10.1016/j.jenvman.2013.06.044

Gaikwad, M. S. & Balomajumder, C. (2017). Simultaneous rejection of chromium(VI) and fluoride [Cr(VI) and F] by nanofiltration: Membranes characterizations and estimations of membrane transport parameters by CFSK model. *Journal of Environmental Chemical Engineering*, *5*(1), 45–53. https://doi.org/10.1016/j.jece.2016.11.018

Garg, V. K., Gupta, R., Kumar, R. & Gupta, R. K. (2004). Adsorption of chromium from aqueous solution on treated sawdust. *Bioresource Technology*, *92*(1), 79–81. https://doi.org/10.1016/j.biortech.2003.07.004

Godinho, D., Dias, D., Bernardo, M., Lapa, N., Fonseca, I., Lopes, H. & Pinto, F. (2017). Adding value to gasification and co-pyrolysis chars as removal agents of Cr3+. *Journal of Hazardous Materials*, *321*, 173–182. https://doi.org/10.1016/j.jhazmat.2016.09.006

Golder, A. K., Chanda, A. K., Samanta, A. N. & Ray, S. (2007). Removal of Cr(VI) from aqueous solution: Electrocoagulation vs chemical coagulation. *Separation Science and Technology*, *42*(10), 2177–2193. https://doi.org/10.1080/01496390701446464

Gopinath, A., Divyapriya, G., Srivastava, V., Laiju, A. R., Nidheesh, P. v. & Kumar, M. S. (2021). Conversion of sewage sludge into biochar: A potential resource in water and wastewater treatment. *Environmental Research*, *194*(May 2020), 110656. https://doi.org/10.1016/j.envres.2020.110656

Guo, H., Bi, C., Zeng, C., Ma, W., Yan, L., Li, K. & Wei, K. (2018). Camellia oleifera seed shell carbon as an efficient renewable bio-adsorbent for the adsorption removal of hexavalent chromium and methylene blue from aqueous solution. *Journal of Molecular Liquids*, *249*, 629–636. https://doi.org/10.1016/j.molliq.2017.11.096

Haktanır, C., Özbelge, H. Ö., Bıçak, N. & Yılmaz, L. (2017). Removal of hexavalent chromium anions via polymer enhanced ultrafiltration using a fully ionized polyelectrolyte. *Separation Science and Technology (Philadelphia)*, *52*(15), 2487–2497. https://doi.org/10.1080/01496395.2017.1343351

Hamadi, N. K., Chen, X. D., Farid, M. M. & Lu, M. G. Q. (2001). Adsorption kinetics for the removal of chromium(VI) from aqueous solution by adsorbents derived from used tyres and sawdust. *Chemical Engineering Journal*, *84*(2), 95–105. https://doi.org/10.1016/S1385-8947(01)00194-2

Haroon, H., Shah, J. A., Khan, M. S., Alam, T., Khan, R., Asad, S. A., Ali, M. A., Farooq, G., Iqbal, M. & Bilal, M. (2020). Activated carbon from a specific plant precursor biomass for hazardous Cr(VI) adsorption and recovery studies in batch and column reactors: Isotherm and kinetic modeling. *Journal of Water Process Engineering*, *38*(March), 101577. https://doi.org/10.1016/j.jwpe.2020.101577

Hayashi, N., Matsumura, D., Hoshina, H., Ueki, Y., Tsuji, T., Chen, J. & Seko, N. (2021). Chromium(VI) adsorption–reduction using a fibrous amidoxime-grafted adsorbent. *Separation and Purification Technology*, *277*(August), 119536. https://doi.org/10.1016/j.seppur.2021.119536

He, R., Yuan, X., Huang, Z., Wang, H., Jiang, L., Huang, J., Tan, M. & Li, H. (2019). Activated biochar with iron-loading and its application in removing Cr (VI) from aqueous solution. *Colloids and Surfaces A: Physicochemical and Engineering Aspects*, *579*(July), 123642. https://doi.org/10.1016/j.colsurfa.2019.123642

Herath, A., Layne, C. A., Perez, F., Hassan, E. B., Pittman, C. U. & Mlsna, T. E. (2021). KOH-activated high surface area Douglas Fir biochar for adsorbing

aqueous Cr(VI), Pb(II) and Cd(II). *Chemosphere*, *269*, 128409. https://doi.org/10.1016/j.chemosphere.2020.128409

Hotová, G., Slovák, V., Zelenka, T., Maršálek, R. & Parchaňská, A. (2020). The role of the oxygen functional groups in adsorption of copper (II) on carbon surface. *Science of the Total Environment*, *711*. https://doi.org/10.1016/j.scitotenv.2019.135436

Hu, L., Wang, P., Zhang, G., Liu, G., Li, Y., Shen, T. & Crittenden, J. C. (2020). Enhanced persulfate oxidation of organic pollutants and removal of total organic carbons using natural magnetite and microwave irradiation. *Chemical Engineering Journal*, *383*(July 2019), 123140. https://doi.org/10.1016/j.cej.2019.123140

Idris, A., Hassan, N., Rashid, R. & Ngomsik, A. F. (2011). Kinetic and regeneration studies of photocatalytic magnetic separable beads for chromium (VI) reduction under sunlight. *Journal of Hazardous Materials*, *186*(1), 629–635. https://doi.org/10.1016/j.jhazmat.2010.11.101

Ioannidou, O. & Zabaniotou, A. (2007). Agricultural residues as precursors for activated carbon production-A review. *Renewable and Sustainable Energy Reviews*, *11*(9), 1966–2005. https://doi.org/10.1016/j.rser.2006.03.013

Islam, M. Azharul, Benhouria, A., Asif, M. & Hameed, B. H. (2015). Methylene blue adsorption on factory-rejected tea activated carbon prepared by conjunction of hydrothermal carbonization and sodium hydroxide activation processes. *Journal of the Taiwan Institute of Chemical Engineers*, *52*, 57–64. https://doi.org/10.1016/j.jtice.2015.02.010

Islam, Md Aminul, Angove, M. J. & Morton, D. W. (2019). Recent innovative research on chromium (VI) adsorption mechanism. *Environmental Nanotechnology, Monitoring and Management*, *12*(July), 100267. https://doi.org/10.1016/j.enmm.2019.100267

Islam, Md Aminul, Angove, M. J., Morton, D. W., Pramanik, B. K. & Awual, M. R. (2020). A mechanistic approach of chromium (VI) adsorption onto manganese

oxides and boehmite. *Journal of Environmental Chemical Engineering*, *8*(2), 103515. https://doi.org/10.1016/j.jece.2019.103515

Jana, S., Purkait, M. K. & Mohanty, K. (2010). Preparation and characterization of low-cost ceramic microfiltration membranes for the removal of chromate from aqueous solutions. *Applied Clay Science*, *47*(3–4), 317–324. https://doi.org/10.1016/j.clay.2009.11.036

Jin, H., Capareda, S., Chang, Z., Gao, J., Xu, Y. & Zhang, J. (2014). Biochar pyrolytically produced from municipal solid wastes for aqueous As(V) removal: Adsorption property and its improvement with KOH activation. *Bioresource Technology*, *169*, 622–629. https://doi.org/10.1016/j.biortech.2014.06.103

Jin, W., Du, H., Zheng, S. & Zhang, Y. (2016). Electrochemical processes for the environmental remediation of toxic Cr(VI): A review. *Electrochimica Acta*, *191*, 1044–1055. https://doi.org/10.1016/j.electacta.2016.01.130

Kanagaraj, G. & Elango, L. (2019). Chromium and fluoride contamination in groundwater around leather tanning industries in southern India: Implications from stable isotopic ratio Δ53Cr/Δ52Cr, geochemical and geostatistical modelling. *Chemosphere*, *220*, 943–953. https://doi.org/10.1016/j.chemosphere.2018.12.105

Karimi-Maleh, H., Ayati, A., Ghanbari, S., Orooji, Y., Tanhaei, B., Karimi, F., Alizadeh, M., Rouhi, J., Fu, L. & Sillanpää, M. (2021). Recent advances in removal techniques of Cr(VI) toxic ion from aqueous solution: A comprehensive review. *Journal of Molecular Liquids*, *329*. https://doi.org/10.1016/j.molliq.2020.115062

Khan, S. R., Zeeshan, M., Khokhar, M. F., Zeshan & Ahmad, I. (2021). A comprehensive study on upgradation of pyrolysis products through co-feeding of waste tire into rice straw under broad range of co-feed ratios in a bench-scale fixed bed reactor. *Biomass Conversion and Biorefinery*. https://doi.org/10.1007/s13399-021-01434-9

Khan, S. R., Zeeshan, M. & Masood, A. (2020). Enhancement of hydrocarbons production through co-pyrolysis of acid-treated biomass and waste tire in a fixed

bed reactor. *Waste Management*, *106*, 21–31. https://doi.org/10.1016/j.wasman.2020.03.010

Kołodyńska, D., Krukowska, J. & Thomas, P. (2017). Comparison of sorption and desorption studies of heavy metal ions from biochar and commercial active carbon. *Chemical Engineering Journal*, *307*, 353–363. https://doi.org/10.1016/j.cej.2016.08.088

Kumar, A. & Jena, H. M. (2017). Adsorption of Cr(VI) from aqueous solution by prepared high surface area activated carbon from Fox nutshell by chemical activation with H3PO4. *Journal of Environmental Chemical Engineering*, *5*(2), 2032–2041. https://doi.org/10.1016/j.jece.2017.03.035

Li, J., Jiang, B., Liu, Y., Qiu, C., Hu, J., Qian, G., Guo, W. & Ngo, H. H. (2017). Preparation and adsorption properties of magnetic chitosan composite adsorbent for Cu2+ removal. *Journal of Cleaner Production*, *158*, 51–58. https://doi.org/10.1016/j.jclepro.2017.04.156

Li, K., Zhang, D., Niu, X., Guo, H., Yu, Y., Tang, Z., Lin, Z. & Fu, M. (2022). Insights into CO2 adsorption on KOH-activated biochars derived from the mixed sewage sludge and pine sawdust. *Science of the Total Environment*, *826*. https://doi.org/10.1016/j.scitotenv.2022.154133

Li, L., Zhang, J., Li, Y. & Yang, C. (2017). Removal of Cr (VI) with a spiral wound chitosan nanofiber membrane module via dead-end filtration. *Journal of Membrane Science*, *544*(March), 333–341. https://doi.org/10.1016/j.memsci.2017.09.045

Li, T., Yang, T., Yu, Z., Xu, G., Han, Q., Luo, G., Du, J., Guan, Y. & Guo, C. (2021). Trivalent chromium removal from tannery wastewater with low cost bare magnetic Fe3O4 nanoparticles. *Chemical Engineering and Processing - Process Intensification*, *169*(30), 108611. https://doi.org/10.1016/j.cep.2021.108611

Li, Y. T., Pi, Y. T., Lu, L. M., Xu, S. H. & Ren, T. Z. (2015). Hierarchical porous active carbon from fallen leaves by synergy of K2CO3 and their supercapacitor performance. *Journal of Power Sources*, *299*, 519–528. https://doi.org/10.1016/j.jpowsour.2015.09.039

Liu, Y., Yang, D., Xu, T., Shi, Y., Song, L. & Yu, Z. Z. (2020). Continuous photocatalytic removal of chromium (VI) with structurally stable and porous Ag/Ag3PO4/reduced graphene oxide microspheres. *Chemical Engineering Journal*, *379*(February 2019), 122200. https://doi.org/10.1016/j.cej.2019.122200

Ma, H. L., Zhang, Y., Hu, Q. H., Yan, D., Yu, Z. Z. & Zhai, M. (2012). Chemical reduction and removal of Cr(VI) from acidic aqueous solution by ethylenediamine-reduced graphene oxide. *Journal of Materials Chemistry*, *22*(13), 5914–5916. https://doi.org/10.1039/C2JM00145D

Ma, H., Yang, J., Gao, X., Liu, Z., Liu, X. & Xu, Z. (2019). Removal of chromium (VI) from water by porous carbon derived from corn straw: Influencing factors, regeneration and mechanism. *Journal of Hazardous Materials*, *369*(October 2018), 550–560. https://doi.org/10.1016/j.jhazmat.2019.02.063

Ma, Y., Qi, Y., Yang, L., Wu, L., Li, P., Gao, F., Qi, X. & Zhang, Z. (2021). Adsorptive removal of imidacloprid by potassium hydroxide activated magnetic sugarcane bagasse biochar: Adsorption efficiency, mechanism and regeneration. *Journal of Cleaner Production*, *292*. https://doi.org/10.1016/j.jclepro.2021.126005

Marzouk, M. A., Elbatal, F. H. & Abdelghany, A. M. (2013). Ultraviolet and infrared absorption spectra of Cr2O3 doped - sodium metaphosphate, lead metaphosphate and zinc metaphosphate glasses and effects of gamma irradiation: A comparative study. *Spectrochimica Acta - Part A: Molecular and Biomolecular Spectroscopy*, *114*, 658–667. https://doi.org/10.1016/j.saa.2013.05.093

Mohamed, A. A. R., El-Houseiny, W., EL-Murr, A. E., Ebraheim, L. L. M., Ahmed, A. I. & El-Hakim, Y. M. A. (2020). Effect of hexavalent chromium exposure on the liver and kidney tissues related to the expression of CYP450 and GST genes of Oreochromis niloticus fish: Role of curcumin supplemented diet. *Ecotoxicology and Environmental Safety*, *188*(November 2019), 109890. https://doi.org/10.1016/j.ecoenv.2019.109890

Mortazavian, S., An, H., Chun, D. & Moon, J. (2018). Activated carbon impregnated by zero-valent iron nanoparticles (AC/nZVI) optimized for simultaneous adsorption and reduction of aqueous hexavalent chromium: Material characterizations and kinetic studies. *Chemical Engineering Journal*, *353*(June), 781–795. https://doi.org/10.1016/j.cej.2018.07.170

Neshat, S. A., Mohammadi, M., Najafpour, G. D. & Lahijani, P. (2017). Anaerobic co-digestion of animal manures and lignocellulosic residues as a potent approach for sustainable biogas production. *Renewable and Sustainable Energy Reviews*, *79*(May), 308–322. https://doi.org/10.1016/j.rser.2017.05.137

Nidheesh, P. v., Scaria, J., Babu, D. S. & Kumar, M. S. (2021). An overview on combined electrocoagulation-degradation processes for the effective treatment of water and wastewater. *Chemosphere*, *263*, 127907. https://doi.org/10.1016/j.chemosphere.2020.127907

Niu, G., Si, C., Jiao, J., Han, Q., Guo, M. & Li, M. (2020). An electron-rich metal-organic framework for highly efficient photocatalytic reduction of Cr(VI). *Journal of Alloys and Compounds*, *830*, 154696. https://doi.org/10.1016/j.jallcom.2020.154696

Pakade, V. E., Tavengwa, N. T. & Madikizela, L. M. (2019). Recent advances in hexavalent chromium removal from aqueous solutions by adsorptive methods. *RSC Advances*, *9*(45), 26142–26164. https://doi.org/10.1039/c9ra05188k

Panda, H., Tiadi, N., Mohanty, M. & Mohanty, C. R. (2017). Studies on adsorption behavior of an industrial waste for removal of chromium from aqueous solution. *South African Journal of Chemical Engineering*, *23*, 132–138. https://doi.org/10.1016/j.sajce.2017.05.002

Pellera, F. M., Giannis, A., Kalderis, D., Anastasiadou, K., Stegmann, R., Wang, J. Y. & Gidarakos, E. (2012). Adsorption of Cu(II) ions from aqueous solutions on biochars prepared from agricultural by-products. *Journal of Environmental Management*, *96*(1), 35–42. https://doi.org/10.1016/j.jenvman.2011.10.010

Qin, Y., Chai, B., Wang, C., Yan, J., Fan, G. & Song, G. (2022). Removal of tetracycline onto KOH-activated biochar derived from rape straw: Affecting

factors, mechanisms and reusability inspection. *Colloids and Surfaces A: Physicochemical and Engineering Aspects*, *640*(November 2021), 128466. https://doi.org/10.1016/j.colsurfa.2022.128466

Qiu, Q., Zhou, M., Cai, W., Zhou, Q., Zhang, Y., Wang, W., Liu, M. & Liu, J. (2019). A comparative investigation on direct carbon solid oxide fuel cells operated with fuels of biochar derived from wheat straw, corncob, and bagasse. *Biomass and Bioenergy*, *121*, 56–63. https://doi.org/10.1016/j.biombioe.2018.12.016

Qu, J., Meng, X., Zhang, Y., Meng, Q., Tao, Y., Hu, Q., Jiang, X., You, H. & Shoemaker, C. A. (2019). A combined system of microwave-functionalized rice husk and poly-aluminium chloride for trace cadmium-contaminated source water purification: Exploration of removal efficiency and mechanism. *Journal of Hazardous Materials*, *379*(December 2018). https://doi.org/10.1016/j.jhazmat.2019.120804

Qu, J., Wang, Y., Tian, X., Jiang, Z., Deng, F., Tao, Y., Jiang, Q., Wang, L. & Zhang, Y. (2021). KOH-activated porous biochar with high specific surface area for adsorptive removal of chromium (VI) and naphthalene from water: Affecting factors, mechanisms and reusability exploration. *Journal of Hazardous Materials*, *401*(June 2020), 123292. https://doi.org/10.1016/j.jhazmat.2020.123292

Ren, G., Wang, X., Huang, P., Zhong, B., Zhang, Z., Yang, L. & Yang, X. (2017). Chromium (VI) adsorption from wastewater using porous magnetite nanoparticles prepared from titanium residue by a novel solid-phase reduction method. *Science of the Total Environment*, *607–608*, 900–910. https://doi.org/10.1016/j.scitotenv.2017.06.103

Rengaraj, S., Yeon, K. H. & Moon, S. H. (2001). Removal of chromium from water and wastewater by ion exchange resins. *Journal of Hazardous Materials*, *87*(1–3), 273–287. https://doi.org/10.1016/S0304-3894(01)00291-6

Sanyal, T., Kaviraj, A. & Saha, S. (2015). Deposition of chromium in aquatic ecosystem from effluents of handloom textile industries in Ranaghat-Fulia region

of West Bengal, India. *Journal of Advanced Research*, *6*(6), 995–1002. https://doi.org/10.1016/j.jare.2014.12.002

Sapari, N., Idris, A. & Hamid, N. H. A. (1996). Total removal of heavy metal from mixed plating rinse wastewater. *Desalination*, *106*(1–3), 419–422. https://doi.org/10.1016/S0011-9164(96)00139-7

Shahrokhi-Shahraki, R., Benally, C., El-Din, M. G. & Park, J. (2021). High efficiency removal of heavy metals using tire-derived activated carbon vs commercial activated carbon: Insights into the adsorption mechanisms. *Chemosphere*, *264*, 128455. https://doi.org/10.1016/j.chemosphere.2020.128455

Shan, R., Shi, Y., Gu, J., Bi, J., Yuan, H., Luo, B. & Chen, Y. (2020). Aqueous Cr(VI) removal by biochar derived from waste mangosteen shells: Role of pyrolysis and modification on its absorption process. *Journal of Environmental Chemical Engineering*, *8*(4), 103885. https://doi.org/10.1016/j.jece.2020.103885

Shi, Yuanji, Zhang, T., Ren, H., Kruse, A. & Cui, R. (2018). Polyethylene imine modified hydrochar adsorption for chromium (VI) and nickel (II) removal from aqueous solution. *Bioresource Technology*, *247*(September 2017), 370–379. https://doi.org/10.1016/j.biortech.2017.09.107

Shi, Yueyue, Shan, R., Lu, L., Yuan, H., Jiang, H., Zhang, Y. & Chen, Y. (2020). High-efficiency removal of Cr(VI) by modified biochar derived from glue residue. *Journal of Cleaner Production*, *254*. https://doi.org/10.1016/j.jclepro.2019.119935

Sivaraman, S., Michael Anbuselvan, N., Venkatachalam, P., Ramiah Shanmugam, S. & Selvasembian, R. (2022). Waste tire particles as efficient materials towards hexavalent chromium removal: Characterisation, adsorption behaviour, equilibrium, and kinetic modelling. *Chemosphere*, *295*(November 2021), 133797. https://doi.org/10.1016/j.chemosphere.2022.133797

Sun, C., Li, C., Wang, C., Qu, R., Niu, Y. & Geng, H. (2012). Comparison studies of adsorption properties for Hg(II) and Au(III) on polystyrene-supported bis-8-oxyquinoline-terminated open-chain crown ether. *Chemical Engineering Journal*, *200–202*, 291–299. https://doi.org/10.1016/j.cej.2012.06.007

Sun, X., Mao, M., Lu, K., Hu, Q., Liu, W. & Lin, Z. (2021). One-step removal of high-concentration arsenic from wastewater to form Johnbaumite using arsenic-bearing gypsum. *Journal of Hazardous Materials*, *424*(PC), 127585. https://doi.org/10.1016/j.jhazmat.2021.127585

Tanhaei, B., Pourafshari Chenar, M., Saghatoleslami, N., Hesampour, M., Laakso, T., Kallioinen, M., Sillanpää, M. & Mänttäri, M. (2014). Simultaneous removal of aniline and nickel from water by micellar-enhanced ultrafiltration with different molecular weight cut-off membranes. *Separation and Purification Technology*, *124*, 26–35. https://doi.org/10.1016/j.seppur.2014.01.009

Wang, C. C., Du, X. D., Li, J., Guo, X. X., Wang, P. & Zhang, J. (2016). Photocatalytic Cr(VI) reduction in metal-organic frameworks: A mini-review. *Applied Catalysis B: Environmental*, *193*, 198–216. https://doi.org/10.1016/j.apcatb.2016.04.030

Wang, C., Li, X., Wu, W., Chen, G. & Tao, J. (2021). Removal of cadmium in water by potassium hydroxide activated biochar produced from Enteromorpha prolifera. *Journal of Water Process Engineering*, *42*(July), 102201. https://doi.org/10.1016/j.jwpe.2021.102201

Wang, W., Ma, X., Sun, J., Chen, J., Zhang, J., Wang, Y., Wang, J. & Zhang, H. (2019). Adsorption of enrofloxacin on acid/alkali-modified corn stalk biochar. *Spectroscopy Letters*, *52*(7), 367–375. https://doi.org/10.1080/00387010.2019.1648296

Wang, Y., Wu, H., Sárossy, Z., Dong, C. & Glarborg, P. (2017). Release and transformation of chlorine and potassium during pyrolysis of KCl doped biomass. *Fuel*, *197*, 422–432. https://doi.org/10.1016/j.fuel.2017.02.046

Wei, X. Z., Gan, Z. Q., Shen, Y. J., Qiu, Z. L., Fang, L. F. & Zhu, B. K. (2019). Negatively-charged nanofiltration membrane and its hexavalent chromium removal performance. *Journal of Colloid and Interface Science*, *553*, 475–483. https://doi.org/10.1016/j.jcis.2019.06.051

Wionczyk, B., Apostoluk, W. & Charewicz, W. A. (2006). Solvent extraction of chromium (III) from spent tanning liquors with Aliquat 336. *Hydrometallurgy*, *82*(1–2), 83–92. https://doi.org/10.1016/j.hydromet.2006.03.055

Wu, Q., Zhang, Y., Cui, M. hua, Liu, H., Liu, H., Zheng, Z., Zheng, W., Zhang, C. & Wen, D. (2022). Pyrolyzing pharmaceutical sludge to biochar as an efficient adsorbent for deep removal of fluoroquinolone antibiotics from pharmaceutical wastewater: Performance and mechanism. *Journal of Hazardous Materials*, *426*(November 2021), 127798. https://doi.org/10.1016/j.jhazmat.2021.127798

WWF, 2020. (2021). Annual Report 2020. *AIMS Allergy and Immunology*, *5*(1), 33–37. https://doi.org/10.3934/allergy.2021003

Xie, Y., Yuan, X., Wu, Z., Zeng, G., Jiang, L., Peng, X. & Li, H. (2019). Adsorption behavior and mechanism of Mg/Fe layered double hydroxide with Fe3O4-carbon spheres on the removal of Pb(II) and Cu(II). *Journal of Colloid and Interface Science*, *536*, 440–455. https://doi.org/10.1016/j.jcis.2018.10.066

Xu, J., Zhang, Y., Li, B., Fan, S., Xu, H. & Guan, D. X. (2022). Improved adsorption properties of tetracycline on KOH/KMnO4 modified biochar derived from wheat straw. *Chemosphere*, *296*. https://doi.org/10.1016/j.chemosphere.2022.133981

Xu, Y., Luo, G., Zhang, Q., Li, Z., Zhang, S. & Cui, W. (2021). Cost-effective sulfurized sorbents derived from one-step pyrolysis of wood and scrap tire for elemental mercury removal from flue gas. *Fuel*, *285*. https://doi.org/10.1016/j.fuel.2020.119221

Yaashikaa, P. R., Senthil Kumar, P., Mohan Babu, V. P., Kanaka Durga, R., Manivasagan, V., Saranya, K. & Saravanan, A. (2019). Modelling on the removal of Cr(VI) ions from aquatic system using mixed biosorbent (Pseudomonas stutzeri and acid treated Banyan tree bark). *Journal of Molecular Liquids*, *276*, 362–370. https://doi.org/10.1016/j.molliq.2018.12.004

Yang, Q., Pan, X., Huang, F. & Li, K. (2010). Fabrication of high-concentration and stable aqueous suspensions of graphene nanosheets by noncovalent

functionalization with lignin and cellulose derivatives. *Journal of Physical Chemistry C*, *114*(9), 3811–3816. https://doi.org/10.1021/jp910232x

Yoon, J., Shim, E., Bae, S. & Joo, H. (2009). Application of immobilized nanotubular TiO2 electrode for photocatalytic hydrogen evolution: Reduction of hexavalent chromium (Cr(VI)) in water. *Journal of Hazardous Materials*, *161*(2–3), 1069–1074. https://doi.org/10.1016/j.jhazmat.2008.04.057

Zhang, H., Shao, J., Zhang, S., Zhang, X. & Chen, H. (2020). Effect of phosphorus-modified biochars on immobilization of Cu (II), Cd (II), and As (V) in paddy soil. *Journal of Hazardous Materials*, *390*(September 2019). https://doi.org/10.1016/j.jhazmat.2019.121349

Zhang, X., Zhang, L. & Li, A. (2018). Eucalyptus sawdust derived biochar generated by combining the hydrothermal carbonization and low concentration KOH modification for hexavalent chromium removal. *Journal of Environmental Management*, *206*, 989–998. https://doi.org/10.1016/j.jenvman.2017.11.079

Zhang, Yanhong, Xu, X., Yue, C., Song, L., Lv, Y., Liu, F. & Li, A. (2021). Insight into the efficient co-removal of Cr(VI) and Cr(III) by positively charged UiO-66-NH2 decorated ultrafiltration membrane. *Chemical Engineering Journal*, *404*(July 2020). https://doi.org/10.1016/j.cej.2020.126546

Zhang, Youwei, Ma, H. L., Peng, J., Zhai, M. & Yu, Z. Z. (2013). Cr(VI) removal from aqueous solution using chemically reduced and functionalized graphene oxide. *Journal of Materials Science*, *48*(5), 1883–1889. https://doi.org/10.1007/s10853-012-6951-8

Zhao, J., Yu, L., Ma, H., Zhou, F., Yang, K. & Wu, G. (2020a). Corn stalk-based activated carbon synthesized by a novel activation method for high-performance adsorption of hexavalent chromium in aqueous solutions. *Journal of Colloid and Interface Science*, *578*, 650–659. https://doi.org/10.1016/j.jcis.2020.06.031

Zhao, J., Yu, L., Ma, H., Zhou, F., Yang, K. & Wu, G. (2020b). Corn stalk-based activated carbon synthesized by a novel activation method for high-performance adsorption of hexavalent chromium in aqueous solutions. *Journal of Colloid and Interface Science*, *578*, 650–659. https://doi.org/10.1016/j.jcis.2020.06.031

Zhao, N., Zhao, C., Lv, Y., Zhang, W., Du, Y., Hao, Z. & Zhang, J. (2017a). Adsorption and coadsorption mechanisms of Cr(VI) and organic contaminants on H3PO4 treated biochar. *Chemosphere*, *186*, 422–429. https://doi.org/10.1016/j.chemosphere.2017.08.016

Zhao, N., Zhao, C., Lv, Y., Zhang, W., Du, Y., Hao, Z. & Zhang, J. (2017b). Adsorption and coadsorption mechanisms of Cr(VI) and organic contaminants on H3PO4 treated biochar. *Chemosphere*, *186*, 422–429. https://doi.org/10.1016/j.chemosphere.2017.08.016

Zhao, Y., Yang, S., Ding, D., Chen, J., Yang, Y., Lei, Z., Feng, C. & Zhang, Z. (2013). Effective adsorption of Cr (VI) from aqueous solution using natural Akadama clay. *Journal of Colloid and Interface Science*, *395*(1), 198–204. https://doi.org/10.1016/j.jcis.2012.12.054

Zhu, Y., Li, H., Zhang, G., Meng, F., Li, L. & Wu, S. (2018). Removal of hexavalent chromium from aqueous solution by different surface-modified biochars: Acid washing, nanoscale zero-valent iron and ferric iron loading. *Bioresource Technology*, *261*(January), 142–150. https://doi.org/10.1016/j.biortech.2018.04.004